Detecting rain-snow-transition elevations in mountain basins using wireless-sensor networks

Guotao Cui[a,*], Roger Bales[a,b], Robert Rice[a], Michael Anderson[c], Francesco Avanzi[b,d], Peter Hartsough[e], Martha Conklin[a]

[a] Sierra Nevada Research Institute and School of Engineering, University of California Merced, Merced, California, USA. [b] Department of Civil and Environmental Engineering, University of California Berkeley, Berkeley, California, USA. [c] California Department of Water Resources, Sacramento, California, USA. [d] CIMA Research Foundation, Savona, Italy. [e] Department of Land, Air, and Water Resources, University of California Davis, Davis, California, USA. * Corresponding author: gcui3@ucmerced.edu

Abstract

To provide complementary information on the hydrologically important rain-snow-transition elevation in mountain basins, this study provides two estimation methods using ground measurements from basin-scale wireless-sensor networks: one based on wet-bulb temperature (T_{wet}), and the other based on snow-depth measurements of accumulation and ablation. With data from 17 spatially distributed clusters (178 nodes) from two networks, in the American and Feather River basins of California's Sierra Nevada, we analyzed transition elevation during 76 storm events in 2014-18. A T_{wet} threshold of 0.5 °C best matched the transition elevation defined by snow depth. Transition elevations using T_{wet} in upper elevations of the basins generally agreed with atmospheric snow level from radars located at lower elevations, while radar snow level was ~100 m higher due to snow-level lowering on windward mountainsides during orographic lifting. Diurnal patterns of the difference between transition elevation and radar snow level were observed in the American, related to diurnal ground-temperature variations. However, these patterns were not found in the Feather due to complex terrain and higher uncertainties in transition-elevation estimates. The American tends to exhibit 100-m higher transition elevations than does the Feather, consistent with the Feather being about 1° latitude further north. Transition elevation averaged 155-m higher in intense atmospheric-river events than in other events, meanwhile, snow-level lowering was enhanced with a 90-m larger difference between radar snow level and transition elevation. On-the-ground continuous observations from distributed sensor networks can complement radar data and provide important ground-truth and spatially resolved information on transition elevations in mountain basins.

Keywords: Rain-snow-transition elevation; Snow level; Wireless-sensor network; Atmospheric river; Mountain basin

1 Introduction

Balancing water storage between headwater snowpack and regolith, versus behind dams, or in groundwater, is central to all aspects of water security, from providing flood protection, to storing water for human and ecosystems use during seasonal and inter-annual dry periods. This is especially important in California given its intense winter storms and Mediterranean climate with wet winters and dry summers. Snowpack in the Sierra Nevada of California and other mountains delays runoff generation by storing winter precipitation in the form of snow and releasing it as snowmelt during spring, thus contributing storage for both water supply and flood control (Bales et al. 2006). Snow cover has large temporal and spatial variability in mountainous regions, related to elevation and other attributes of their complex topography. Knowing the area within a basin at which it is raining or snowing, that is knowing precipitation phase across mountain basins, is thus critical to water-resources decision making. For example, rain-on-snow events with a higher transition elevation and antecedent ground snowpack could enhance flood risk since the snowmelt contributes additional runoff to rainfall totals (Musselman et al. 2018; White et al. 2019).

The rain-snow-transition zone is the elevation range where cold-season precipitation is a mix of rain and snow, with its upper boundary being all snow, and the lower boundary being all rain. The rain-snow-transition elevation is approximately the center of the transition zone, which means that the dominant precipitation phase is snow above and rain below (Figure 1a). The transition elevation and zone can be determined using the phase of precipitation, which depends on temperature. By considering humidity (Harpold et al. 2017; Jennings et al. 2018), and deriving wet-bulb temperature (T_{wet}) (Cleave et al. 2019; Ding et al. 2014; Behrangi et al. 2018; Olsen 2003; Sims and Liu 2015; Zhong et al. 2018) and dewpoint temperature (T_{dew}) (Jennings and Molotch 2019; Marks et al. 2013; Zhang et al. 2017a) one can improve the prediction of precipitation phase, compared to traditional air temperature (T_{air}) alone. As T_{wet} can represent the cooling effects due to evaporation of falling hydrometeors, it is recommended by an increasing number of studies (Wang et al. 2019; Tamang et al. 2020) and used in operational applications, by the National Weather Service (NWS) Western Region (WR) (Cleave et al. 2019). Therefore, the transition elevation and zone can be determined using T_{wet} thresholds for all rain, rain-snow-transition, and all snow in mountain basins (Figure 1a).

The on-the-ground rain-snow-transition elevation can be inferred from remotely sensed observations of atmospheric snow level (i.e. the atmospheric elevation at which snow becomes the dominant form of precipitation). Frequency-Modulated Continuous Wave (FMCW) radars (Johnston et al. 2009, 2017) can

estimate the snow level above their locations by identifying the elevation of the maximum reflectivity in a bright band (White et al. 2002, 2010). Currently, there are 11 FMCW radars in California (https://psl.noaa.gov/data/obs/datadisplay/). Among these, 10 radars were deployed by the National Oceanic and Atmospheric Administration (NOAA)'s Hydrometeorology Testbed - West (HMT-West) project, and the eleventh radar in the coastal mountains west of Santa Clara Valley was recently deployed by the Advanced Quantitative Precipitation Information (AQPI) project. Nine of the 10 radars from the HMT-West project are located near major reservoirs, and the remaining one is located along the Klamath River in northern California (White et al. 2013; Johnston et al. 2017). The vertically pointing S-band FMCW radars can observe to 10 km above the radars at a 40-m vertical resolution (Johnston et al. 2017). These radar-snow-level data are available to forecasters for near-real-time operations. The estimated snow level is typically near the center of the bright band, which is the melting layer, with a thickness of several hundred meters (Figure 1b). The transition between snow and rain occurs within the melting layer. The snow-level height from the FMCW radar was found to be close to the height of the temperature at which the probability of precipitation falling as snow is 50% (Mizukami et al. 2013). The radar snow level observed from the bright band is often ~100-300 m below the elevation of freezing level at 0 ºC T_{air} isotherm (White et al. 2002; Minder et al. 2011; Minder and Kingsmill 2013; Mizukami et al. 2013; Neiman et al. 2013; Cannon et al. 2017; Henn et al. 2020; Sumargo et al. 2020), which can be obtained from numerical weather models, e.g. Weather Research and Forecasting (WRF) model. The radar snow level has been reported to be at T_{air} between 0 and 3 °C (Lundquist et al. 2008; White et al. 2010). The FMCW radar can capture the evolution of snow level, as demonstrated by winter-season data showing that atmospheric snow level near Lake Oroville varied in a range of 600-3200 m (Matrosov et al. 2017). These FMCW radars provide high-temporal-resolution (e.g. 10-minute or 15-minute) snow-level data, which are not readily available from satellite observations (Cannon et al. 2017) or numerical models (Henn et al. 2020; Sumargo et al. 2020), that need to account for the difference between radar snow level and modeled 0 ºC T_{air} isotherm.

Compared to free air upwind, the freezing level and radar snow level on the windward side of the mountains lower with orographic lifting. Marwitz (1983, 1987) found that the freezing level and radar snow level descend during orographic storms over the windward slopes in the Sierra Nevada. Medina et al. (2005) also found lowering of the snow level immediately adjacent to windward slopes of the European Alps and the Oregon Cascades. Semi-idealized modeling (Minder et al. 2011) showed the freezing level intersecting the windward slope of mountains lowering by hundreds of meters compared to its elevation in the free air upwind, due to colder temperature caused by adiabatic cooling of rising air, latent cooling from melting precipitation, and larger frozen-hydrometeor melting distance during the orographic lifting. The freezing-level lowering often occurs near mountainsides and over short horizontal distances (Medina et al. 2005; Minder and Kingsmill 2013). The observed or modeled freezing level, minus an offset, is often used as an approximation of the radar snow level (Mizukami et al. 2013; Henn et al. 2020), which is used for operational streamflow forecasting (Lundquist et al. 2008). Aside from the freezing level, Lundquist et al. (2008) compared the rain-snow-transition elevation using T_{air} of 1.5 °C in the North Fork American River basin to the atmospheric snow level from radar, and suggested that radar bright-band height needs to be adjusted to better match on-the-ground transition elevations.

For estimating the rain-snow-transition elevation, an alternative to remote-sensing platforms is on-the-ground recording of phase-related measurements like T_{air}, relative humidity, and snow depth. The spatial density of operational measurements is typically low at high elevations, which complicates the detection of the rain-snow-transition elevation. Recently installed wireless-sensor networks in the American and Feather River basins provide valuable ground measurements that can be used to test how a denser network could improve detection of the rain-snow-transition elevation. These clusters are strategically deployed across a wide elevational range in mixed rain-snow areas, and capture the spatial variability of physiographic attributes that affect snow accumulation and ablation, e.g. elevation, aspect, slope, and canopy cover (Welch et al. 2013). Compared to traditional operational measurements, distributed sensor-network clusters record dense spatial and temporal measurements of temperature, relative humidity, snow depth, and other attributes that can be used to investigate mountain precipitation and the rain-snow transition (Malek et al. 2017, 2019; Zhang et al. 2017a,b).

Detecting the rain-snow-transition zone is particularly important for atmospheric rivers, which contribute up to 50% of the annual precipitation in California (Dettinger et al. 2011). An atmospheric river

is a long and narrow corridor of water-vapor flux in the lower troposphere, located in the warm sector of extratropical cyclones (Zhu and Newell 1994; Ralph et al. 2004). Atmospheric rivers transport considerable amounts of moisture, and can lead to copious precipitation, enhanced runoff, and flooding (Neiman et al. 2011; Zagrodnik et al. 2018; Ralph et al. 2019), especially because the freezing level is at high elevation when an atmospheric river occurs (Neiman et al. 2011; Zagrodnik et al. 2018). As it is projected that the atmospheric-river events will increase in the future (Gao et al. 2015; Goldenson et al. 2018), the characteristics of the on-the-ground rain-snow-transition elevation during atmospheric-river events, including snow-level lowering, are examined in this study.

The purpose of this work is to examine how wireless-sensor networks can contribute to reliably estimating the rain-snow-transition elevation in mountain basins. Our specific aims are to i) estimate the transition elevation and zone during storm events using dense basin-scale ground measurements of T_{air} and humidity, ii) employ spatial patterns of ground-measured snow accumulation and ablation to derive transition elevation, which is used to analyze temperature thresholds, iii) explore the difference between the on-the-ground transition elevation estimated from the ground T_{wet} and atmospheric snow level from radar, and iv) analyze the transition elevation and its difference relative to radar snow level during atmospheric-river events.

2 Methods

We used ground-based T_{wet} thresholds to determine the precipitation phase during 76 storms in Water Years (WY, 1 October-30 September) 2014-18 in the American and Feather River basins, in California's Sierra Nevada. Wireless-sensor networks in the two basins, consisting of 178 sensor nodes arranged in 17 clusters, provided continuous measurements of T_{air}, relative humidity, and snow depth. At each sensor node, T_{wet} was solved iteratively using T_{air} and relative humidity. At an hourly time step, a linear regression was used to spatially distribute T_{wet} across each mountain basin. The transition elevation was then determined as the elevation where T_{wet} is equal to the rain-snow-transition threshold. Spatial patterns of snow-depth increment and decrement were also used to provide an independent estimate of the ground transition elevation. The T_{wet}- and snow-depth-based transition elevations were compared against the atmospheric snow levels detected by FMCW radar. Atmospheric-river events were identified using Integrated water-Vapor Transport (IVT) (Goldenson et al. 2018; Ralph et al. 2018).

2.1 Study areas

The American and Feather River basins are on the western slope of the Sierra Nevada (Figure 2). The two river basins contribute significant flows to the Sacramento River, and are important for hydropower generation, aquatic ecosystems, downstream agriculture, and municipal water supplies. The two basins have experienced winter extreme-precipitation events associated with land-falling atmospheric rivers, for example, the event in January 1997 for the American River basin (Ohara et al. 2011; Yigzaw et al. 2013) and the event in February 2017 for the Feather River basin (White et al. 2019). Information on rain-snow-transition elevation during extreme-precipitation events is critical for flood-risk management and water-resource planning in the two basins.

The area above Folsom Dam in the American is 4780 km^2, and elevation ranges from 200 m at the Folsom reservoir to 3100 m at the basin crest. Water flows through three major river forks (North, Middle, and South) into Folsom reservoir. In the American, 13 strategically placed sensor clusters (Table 1) were deployed above the average historical snow line of 1500 m (Welch et al. 2013). The sensor network covered the main snowmelt-producing part of the basin, across an elevation range between 1510 and 2723 m and an area of 2080 km^2 (44% of the basin). Each strategically placed cluster contained 10 wireless-sensor nodes, measuring T_{air}, relative humidity, snow depth, soil moisture, and solar radiation at 15-min intervals.

The Feather River basin has an area of 9430 km^2 above Oroville Dam, with elevations ranging from 280 m at the dam to over 2700 m at the crest. Four sensor clusters were deployed above the average historical snow line of 1600 m (Risley et al. 2011; Koczot et al. 2004), covering a 1697-2277 m range in elevation, which includes 3560 km^2 (76%) of the basin. Each of the clusters in the Feather has 12 sensor nodes, which record the same measurements as those in the American (Malek et al. 2017). However, mixed arrangements of ridges and valleys form a complex topography in the Feather, where significantly more precipitation is received on the western side than in the rain-shadowed eastern side (Koczot et al. 2004; Freeman 2011). Two clusters (HMB and BKL) were placed on the western side of the basin, while the other two clusters (KTL and GRZ) in the eastern, rain-shadow area (Table 1).

2.2 Data

The 15-min-interval T_{air}, relative-humidity, and snow-depth measurements from the wireless-sensor networks (Table 1) were averaged to develop hourly products at each node. Data were available for WY 2014-17 in the

American and WY 2017-18 in the Feather, reflecting the later deployment of sensors in the Feather. During WY 2014-18, these basins and California as a whole experienced hydroclimate extremes (Hatchett et al. 2017), including the drought years culminating in critically warm and dry 2015 (5% of the historical April 1 snowpack), and the wettest year for the basins, 2017 (159% of the historical April 1 snowpack). Field data were processed and gaps filled as described previously (Zhang et al. 2017a; Bales et al. 2018; Bales et al. 2020).

Atmospheric snow-level products from National Oceanic and Atmospheric Administration (NOAA) were from two FMCW radars (10-min), one near the Feather at Oroville (39.532° N, 121.488° W, 114 m elevation), and one near the American at Colfax (39.080° N, 120.938° W, 644 m elevation) (Figure 2). The two FMCW radars are part of a statewide network of ground-based instrumentation designed to monitor the impacts of landfalling storms with atmospheric rivers (White et al. 2013). This network was installed and is operated and maintained with funding provided by the California Department of Water Resources. The processed snow-level data from the two FMCW radars were acquired from the Earth Systems Research Laboratory (http://www.esrl.noaa.gov) and averaged to an hourly resolution.

Storms in WY 2014-17 were selected based on precipitation measured at 4 operational precipitation gauges in the American River basin (Table 1 and Figures 2-3), and storms in WY 2018 were selected based on 4 precipitation gauge data in the Feather River basin. The storms in WY2017 selected using gauge data in the American were also used for the Feather (Figure S1). The operational precipitation gauges data were downloaded from the California Data Exchange Center (CDEC, http://cdec.water.ca.gov). The IVT at basin outlets was obtained from the Modern-Era Retrospective analysis for Research and Applications, Version 2 (MERRA-2, produced by NASA's Global Modeling and Assimilation Office, https://gmao.gsfc.nasa.gov, Gelaro et al., 2017). The IVT (kg m^{-1} s^{-1}) is a measure of the direction and intensity of water flux in an atmospheric column, which is the key to defining and categorizing atmospheric rivers (Ralph et al. 2018, 2019). We selected 76 storms in WY 2014-18, during which the cumulative precipitation from the operational precipitation gauges was larger than 2 cm in consecutive precipitation days. To identify atmospheric-river events making landfall in our study areas, we analyzed the moisture fluxes from the MERRA-2 dataset to visually detect a long (> 2000 km) and narrow (< 1000 km) corridor with IVT larger than 250 kg m^{-1} s^{-1}, to ensure that the atmospheric river intersected the northern Sierra Nevada (Demaria et al. 2017; Ralph et al. 2018). The manually classified events were further verified by an automatic atmospheric-river-detection algorithm using hourly MERRA-2 reanalysis data (Goldenson et al. 2018). For WY 2017, 24 precipitation events were selected based on the above criteria (Figure 3). Eighteen events were classified as atmospheric-river related, associated with IVT above 250 kg m^{-1} s^{-1} (Figure 3f). The remaining 6 events were non-atmospheric-river-related, i.e. no atmospheric-river landfalling was observed. Snow-level data from FMCW radars were evaluated during periods when precipitation gauges recorded precipitation. The low radar snow levels in August 2017 were not accompanied by noticeable precipitation or a strong IVT in the atmosphere.

2.3 Rain-snow-transition elevation

To determine the rain-snow-transition elevation, ground measurements from the wireless-sensor networks were used by two independent methods, one based on a T_{wet} threshold, and the other based on the spatial pattern of snow-depth changes (Figure 4).

As T_{wet} was not directly measured by the wireless-sensor networks, we first calculated hourly T_{dew} at each sensor node using measured T_{air} and relative humidity by an empirical equation (Lawrence 2005; Zhang et al. 2017a). Then T_{wet} at each sensor node was iteratively derived by T_{air} and T_{dew} using the psychrometric equation (Marks et al. 2013), following the algorithm in iSnobal model from the Spatial Modeling for Resources Framework (SMRF; https://github.com/USDA-ARS-NWRC/smrf). Since the sensor nodes covered a large elevation range of the basin, we established a linear regression between T_{wet} and elevation at an hourly step. Then the transition zone was estimated as the elevations where T_{wet} is between snow and rain thresholds based on the regression (Figures 1a and 4). Precipitation was assumed to be a proportional mix of rain and snow within the transition zone. The transition elevation on the ground was determined as the elevation of T_{wet} at the threshold for rain-snow transition, with snowfall more than rainfall above, and rain dominating below (Figure 1a). The lapse rate of T_{wet} is the regression slope using the hourly data, which means that T_{wet} changes along the elevation gradient. Therefore, the transition elevation and T_{wet} lapse rate for each storm event were investigated at 1-hour intervals.

This study also developed an independent method to derive transition elevation using the spatial patterns of ground-measured snow-depth changes from distributed sensor networks. As the sensors measure snow accumulation and ablation along elevation gradients, we

can derive the rain-snow-transition elevation by an iterative algorithm. This approach assumed that decreases in snow depth were caused by rain on snow, with snow-depth increases representing snowfall, neglecting snowmelt and redistribution during winter storms. For example, Figure 5b shows the snow-depth changes during a storm in February 2014 in the American. The spatial patterns of snow-depth changes reflected the rain-snow-transition elevation, as snow depth increased above the transition and decreased below. Therefore, for a test elevation (z) within the elevation coverage of the sensor network, the iterative algorithm minimizes the summation ($F(z)$) of total snow-depth decrement ($SDD(z)$) at the sensor nodes above z and the total snow-depth increment ($SDI(z)$) at the sensor nodes below z. The algorithm for snow-depth-derived transition elevation is shown in equations (1-2),

$$F(z) = SDD(z) + SDI(z) \quad (1)$$

$$Snow\text{-depth-}derived\ transition\ elevation = min\ F(z) \quad (2)$$

The ground snow-depth-derived transition elevation was used to analyze the appropriate T_{wet} threshold of the transition elevation. Previous researchers (Cleave et al. 2019) found the highest likelihood of mixed rain and snow between elevations corresponding to T_{wet} of 0 and 1 °C, and defined the snow level as the elevation with T_{wet} of 0.5 °C. This suggested that thresholds of all snow above 0 °C, equal rain and snow at 0.5 °C, and all rain below 1 °C for the T_{wet}-based approach (Figure 1a). Since the ground snow-depth-derived transition elevations were obtained independently (Figure 5b), they were used to compare to results from different temperature thresholds (Figure 5a), such as thresholds of ±1 °C (Zhang et al. 2017a), ±0.5 °C (Marks et al. 2013), and 1.5 °C (Lundquist et al. 2008). In doing so, appropriate T_{wet} thresholds can be selected and then used in estimating transition elevations.

With the transition elevations estimated using T_{wet} thresholds, we can calculate basin-scale potential runoff and snowpack volume to investigate the importance of atmospheric-river events versus non-atmospheric-river events. The gridded daily precipitation product Parameter-elevation Relationships on Independent Slopes Model (PRISM) at 800-m spatial resolution (Daly et al., 2008) was used in this study. For the two basins, the calculation was performed in 50-m elevation bins. For each day during storm events, the rainfall and snowfall amounts were determined by the transition elevation with an assumption of linear snow fraction in the transition zone. The potential runoff volume was calculated as the rainfall depth multiplied the corresponding rainfall area. In a similar manner, the potential snowpack volume was determined as the snowfall (water equivalent) depth multiplied the corresponding snowfall area.

3 Results

3.1 T_{wet} thresholds from ground snow-depth-derived transition elevation

Since the wireless-sensor network in the American had a larger elevational coverage and more measurements than that in the Feather, the daily rain-snow-transition elevations derived from snow accumulation and ablation in the American were compared to results from different T_{wet} thresholds and radar snow level (Table 2 and Figure 6), for periods when patterns of snow-depth increment or decrement were confidently differentiated within the elevation range of the sensor nodes. Results of Root Mean Squared Difference (RMSD), mean difference, and percent (mean) difference in Table 2 showed that the rain-snow-transition elevation using T_{wet} threshold of 0.5 °C provided most agreement to the snow-depth-based transition elevation (Figure 6a), with RMSD of 155 m, mean difference of 21 m, and percent difference of 1.0%. Radar snow levels were higher than transition elevations derived from snow depth (Figure 6b), with RMSD of 372 m, mean difference of 272 m, and percent difference of 13.3%. Therefore, T_{wet} of 0.5 °C was chosen as the threshold for the rain-snow-transition elevation.

T_{wet} thresholds of 0 °C and 1.0 °C did not match snow-depth changes as well (mean difference of 110 and -69 m, respectively) but were chosen as the thresholds for all snow above and all rain below, respectively, to define the transition zone. These T_{wet} thresholds were the same as estimated from 10-years of surface-precipitation-type observations and sounding balloons in a rain-versus-snow study (Cleave et al. 2019). A similar T_{wet} threshold (0.3 °C) corresponding to the radar snow level was indicated based on the sounding temperature and radar-bright-band-height measurements for 5 winters in California (Lundquist et al. 2008).

3.2 Evolution of rain-snow-transition elevation during storm events

To demonstrate the capability of wireless-sensor networks to track the evolution of the on-the-ground rain-snow transition during storms, two events for the American and Feather basins are shown as examples.

For the American, the event during December 18-24, 2015 was associated with an atmospheric river. The precipitation gauge at BTP recorded more than 5 cm of precipitation on December 20 (Figure 7f) and snow depth at some sensor nodes increased over 40 cm (Figures 7e and 7g). The estimated rain-snow-transition

elevation from the ground T_{wet} correlated well with the radar-detected snow level during this storm, with a correlation coefficient (r) of 0.74 and RMSD of 352 m (Figure 7a). During snowfall detected by the radar, the lapse rate for T_{wet} averaged –4.3 °C km^{-1} (Figure 7b), and the coefficient of determination (r^2) of the linear regression between T_{wet} and elevation was high (0.86, Figure 7c). Meanwhile, the width of 95% confidence interval averaged 93 m, which was narrower than the mean 209-m thickness of the transition zone (black-dotted lines and shaded areas in Figure 7a). T_{air} was close to T_{wet} and T_{dew} during precipitation (Figures 7d and 7h), indicating that the air was close to saturation. Basin-averaged T_{wet} showed a similar evolution pattern to that for the transition elevation (r = 0.95) and radar snow level (r = 0.84), indicating that the evolution of transition elevation was closely related to the evolution of basin-scale T_{wet}. The estimated transition elevation agreed with the temporal changes of measured snow depths and evolved during the storm. There was a slight snow-depth increase at most nodes on December 18, 19, and 23, associated with the low rain-snow-transition elevation. On December 20 and 21, a category-scale 2 atmospheric river made landfall in the American River basin (Ralph et al. 2019), as the peak of IVT at Folsom Dam was 675 kg m^{-1} s^{-1} and duration of IVT > 250 kg m^{-1} s^{-1} was 45 hours. Consequently, the basin received more precipitation on these two days. The temperature increased during this period since the basin was in the warm sector of the cyclone, which led to a higher transition elevation on December 21. About half of the sensor nodes, mainly above 2000 m elevation, recorded an increase of snow depth, indicating fresh snow on December 21 (Figures 7e and 7g). In contrast, the lower-elevation nodes recorded decreasing snow depths, since the rainfall melted and consolidated the snowpack. The snow-depth-derived ground transition elevation for December 21 was 2005 m, which was higher than the 1750 m from T_{wet} and lower than the radar snow level of 2140 m. In this case, the radar snow level was closer to snow-depth-derived transition elevation, while the difference between the T_{wet}-based transition elevation and the radar snow level was large (390 m), highlighting the important role of ground snow depth as a complementary evaluation.

The evolution of the rain-snow transition during a non-atmospheric-river event in March 2018 can be illustrated using data from the Feather. During this event on March 13-17, 2018, snow depths at the 4 sensor clusters increased by over 50 cm (Figures 8e and 8g), with accumulated precipitation of about 8 cm (Figure 8f). The ground-based rain-snow transition and snow level from the radar at Oroville coincided well (r = 0.94), and remained below 1600 m after March 13 (Figure 8a), since the T_{wet} at the lowest sensor node was below 0 °C (Figure 8d). However, the two very low radar snow levels (i.e. 824 and 627 m) on March 12 appear to be outliers, since the subsequent radar-detected snow levels were around 2500 m, and were associated with high T_{wet} values. The RMSD between the radar snow level without the outliers and the ground-based rain-snow transition was 170 m. During the four snow days, the difference between T_{air} and T_{wet} at the nodes was less than 0.05 °C (Figure 8d), the difference between T_{air} and T_{dew} was less than 0.1 °C, indicating the air was saturated (Figure 8h). During snowfalls, the mean coefficient of determination (r^2) between hourly T_{wet} and node elevation was above 0.81, suggesting a strong linear relationship (Figure 8c). Meanwhile, the width of the 95% confidence interval averaged 176 m, which was slightly wider than the mean thickness of the transition zone 170 m (Figure 8a). The mean (± standard deviation) lapse rate for T_{wet} was –5.2±2.1 °C km^{-1} (Figure 8b).

3.3 On-the-ground rain-snow-transition elevation versus atmospheric snow level

Figure 9 shows the comparison between the hourly on-the-ground rain-snow transition elevation from sensor networks and radar snow level in the American and Feather River basins during the storm events from November to April in WY 2014-18. For the American (Figure 9a), the transition elevation agreed well with the radar-detected snow level (r = 0.84 and RMSD = 305 m). Compared to radar snow levels, the transitions elevation from T_{wet} showed lower estimates, with percent (mean) differences of –4.9 and –6.4% (–91 and –118 m) in the American and Feather, respectively. The best-fit slopes for both basins are similar, 1.10 and 1.15 for the American and Feather, respectively. The ground-based sensor network showed a lower rain-snow transition than did the radar (Figure 9).

In the Feather with fewer sensor clusters, a similar agreement between the ground-based and radar snow levels was found (r = 0.86 and RMSD = 384 m). In general, most scatter points in Figure 9 followed the regression line, and there were some outliers in the radar-detected snow-level data, e.g. the snow level on March 12, 2018 in Figure 8a.

The on-the-ground rain-snow-transition elevation and radar snow level in common WY 2017 were compared between the American and Feather (Figure 10). The American had a 102-m higher on-the-ground rain-snow-transition elevation (6.0%) (Figure 10a), and a 63-m higher radar snow level (Figure 10b). The best-fit slopes

were 0.93 and 0.92 (less than 1) for on-the-ground transition elevation and radar snow level, respectively.

The probability densities of the rain-snow-transition and land-surface elevations for the two basins, and hypsometric curves, are shown in Figure 11. For the American, over WY 2014-17 80% of the transition elevations were above 1440 m, meaning that areas below 1440 m would not receive snow during 80% of snowfall time (detected by radar snow level) during winter storms. The mean value was 1800 m. For the 2710 km^2 (56%) of the basin below 1500 m, they generally (more than 74% of the time) did not receive snow during storms (Figures 11a and 11b). The American River basin has a 64% chance that the transition elevation lies within 1400-2200 m (one standard deviation from the mean). For the Feather, the median snow level was 1700 m using the data over WY 2017-18. However, 80% of the snow levels in the Feather were above a lower elevation of 1230 m, and a lower mean of 1720 m, compared to the American. Moreover, the Feather had a wider elevation range for the transition, also indicated by the larger standard deviation in the Feather (500 m) than the American (400 m). The chance of the transition elevation in the Feather located between 1200 and 2250 m (one standard deviation away from its mean) was 64%, and 50% chance between 1400 and 2200 m. Since the distribution of surface elevation in the Feather spans a narrow range, snowfall would cover 81% (7670 km^2) of the basin area, for a transition elevation of 1230 m (Figures 11c and 11d). However, there is a 32% chance that 90% (8490 km^2) of the basin area would not receive snow when the snow level is above 1990 m, as the Feather has a small fraction of area in high elevations.

3.4 Transition zone and lapse rate of T_{wet}

The thicknesses of the rain-snow-transition zone using a threshold window between 0 and 1 °C and the lapse rate of T_{wet} are shown in Figure 12. For the American, the mean (±standard deviation) of the T_{wet} lapse rate is –4.7±1.3 ºC km^{-1}, with a transition-zone thickness of 180±30 m (Figures 12a and 12c). Corresponding values for the Feather are –5.3±1.9 ºC km^{-1} and 180±55 m. Thus, the Feather had a larger variance for both the T_{wet} lapse rate and transition-zone thickness, compared to the American. For both basins, there is more than a 66% chance that the values of both attributes would fall within one standard deviation of their means. The larger mean thickness of the transition zone in the American reflects its higher observed T_{wet} lapse rate. The width of the 95% confidence interval for the regression of rain-snow-transition elevation at T_{wet} = 0.5 °C (e.g. Figures 7a and 8a) are 90±40 m and 110±80 m for the American and Feather, respectively, which are narrower than their corresponding thicknesses of the transition zone (Figure 12b). The widths of confidence interval typically correspond to T_{wet} differences of 0.4 and 0.6 °C for the American and Feather, respectively. The higher uncertainties in transition elevation estimates in the Feather were expected, as only 4 clusters were used for T_{wet} regression, compared to 13 clusters in the American. Besides the fewer clusters, 2 of the 4 clusters are located in eastern rain-shadow areas in the Feather (Figure 2), leading to higher uncertainties.

3.5 Transition elevation and potential runoff during atmospheric-river events

Figure 13 shows the event-averaged rain-snow-transition elevation, mean IVT intensity, basin-averaged T_{air}, and daily basin-averaged snow-depth increment for atmospheric-river versus non-atmospheric-river events in the two basins. As expected, events with higher T_{air} were associated with a higher transition elevation. This was also indicated by the positive correlation between the event-averaged transition elevation from the sensor network and basin-averaged daily T_{air} during an entire storm event (Figures 13a and 13b), with r = 0.59 for the American (WY 2014-17) and r = 0.85 for the Feather (WY 2017-18). For the common wet WY 2017, correlations for the American and Feather were 0.72 and 0.81, respectively. The higher correlation in the Feather is due to a higher mean relative humidity of 91%, compared to that of 83% in the American, since T_{air} is closer to T_{wet} when the air approaches saturation. Note that if averaging hourly T_{air} only during snowfall periods of each storm, T_{air} can explain the 87% and 92% variance of transition elevation (not shown), respectively, for the American and Feather.

For 52 winter events in WY 2014-17 in the American (Figure 13a), 36 events were associated with atmospheric rivers and had mean IVT intensities significantly larger than those from non-atmospheric-river events (p-value of one-way ANOVA is 0.00003). Half of the events had a rain-snow-transition elevation between 1530-1950 m (25th-75th percentiles). Atmospheric-river-related events tended to have a 160-m higher rain-snow transitions than did non-atmospheric-river events (p = 0.08). Basin-averaged snow-depth increments were negatively related to the rain-snow elevation, with r = –0.48. Although atmospheric-river-related events in the American were associated with more-intense precipitation, basin-averaged snow-depth increments between non-atmospheric-river versus atmospheric-river events show no statistically significant difference (p = 0.17).

In a similar manner, for 35 winter events in WY 2017-18 in the Feather, 25 (71%) atmospheric-river-related events have a larger mean IVT intensity and a 150-m higher event-averaged transition elevation than non-atmospheric-river events (Figure 13b). The 25th percentile of the transition elevation was 1410 m and the 75th percentile was 2100 m. The transition elevation was negatively correlated to basin-averaged snow-depth increment ($r = –0.64$). Again, the differences in basin-averaged snow-depth increments between non-atmospheric-river and atmospheric-river events were not significant ($p = 0.55$), notwithstanding that gauge precipitation was significantly larger in atmospheric-river events ($p = 0.07$).

Figure 14 shows the comparison of the impacts of wintertime atmospheric-river events and non-atmospheric-river events on potential runoff and snowpack volume using the gridded PRISM dataset. For the two basins, the mean daily basin-averaged precipitation during the atmospheric-river events was significantly larger (~13 mm) than during non-atmospheric-river events (Figures 14b and 14f), due to larger IVT intensity associated with atmospheric rivers. Larger proportions of rain area were shown during atmospheric-river events (Figures 14a and 14e), since the atmospheric-river events have a higher transition elevation caused by warmer temperature. The difference of rain area between atmospheric-river events and non-atmospheric-river events was more pronounced in the Feather (21%) than in the American (12%), which can be explained by the fact that the substantially larger proportion of the Feather is often in the transition elevation (Figure 11). For both basins, the potential runoff volume was significantly larger during the atmospheric-river events (Figures 14d and 14h), indicating a greater contribution to reservoir inflow, than during the non-atmospheric-river events. As the Feather is twice the area of the American, the difference of daily potential runoff volume between atmospheric-river events and non-atmospheric-river events was more prominent in the Feather ($1.05 \times 10^7\ m^3$) than in the American ($0.59 \times 10^7\ m^3$). However, in terms of the potential snowpack from snowfall (Figures 14c and 14g), the differences between atmospheric-river events and non-atmospheric-river events were not statistically significant ($p=0.085$ and 0.416 for the American and the Feather, respectively). This is consistent with the above results that no significant difference of basin-averaged snow-depth increment between these two kinds of storm events (Figure 13), revealing the higher rain-snow-transition elevation diminishes the benefits of snowfall with more considerable precipitation during atmospheric rivers.

Aggregating all the wintertime events showed that atmospheric-river events contributed 86% and 85% of total precipitation for the American and the Feather, respectively. Regarding the total potential runoff, atmospheric-river events contributed 88% and 89% for the American and the Feather, respectively, which were slightly larger than their contributions to the total precipitation. In contrast, atmospheric-river events had relatively lower contributions of 81% and 73% to total potential snowpack, respectively, for the American and the Feather.

4 Discussion

4.1 Variabilities of rain-snow-transition elevation and zone

The rain-snow-transition elevation in mountains varies at hourly and event time scales (Figures 7, 8, and 13). On an event scale, the event-averaged T_{air} and IVT intensity both positively affect the transition elevation (Figure 13). Using multiple linear regression, event-averaged T_{air} and IVT intensity explained 48% and 76% of the transition-elevation variance for the American and the Feather, respectively. At an hourly time scale, T_{air} is close to T_{wet} during precipitation periods, since relative humidity is comparatively high when precipitation occurs. The hourly T_{air} can satisfactorily explain the temporal variation of the transition elevation ($r^2 > 87\%$). Therefore, fine-time-scale T_{air} can better indicate the transition than using coarse-scale data, as the transition elevation can rapidly change in response to meteorological conditions.

Analysis of the on-the-ground data for the 76 events indicates that atmospheric-river events tend to show higher transition elevations than non-atmospheric-river events. This atmospheric-river effect on rain-snow transition observed from on-the-ground data is explained by the warmer conditions coming with winter landfalling atmospheric rivers, leading to higher freezing levels (Neiman et al. 2008). For the atmospheric-river events, the basin-averaged snow-depth increment is not significantly higher than those in non-atmospheric-river events, because of melting and consolidating snow in lower elevations when transition elevation is higher. This reflects higher transition elevations during atmospheric-river events, leading to less snowfall and at times resulting in rain-on-snow events at lower elevations. Along with the intense precipitation during atmospheric-river events (Huning et al. 2019; Lettenmaier 2019), the additional snowmelt with

warmer conditions enhances runoff and can increase the threat of flooding.

The thickness of the transition zone is ~180±40 m in the two basins, as determined by the T_{wet} lapse rate of about –5 ºC km^{-1} with thresholds of 0 and 1 °C during snowfall periods. For reference, Feld et al. (2013) found median T_{dew} lapse rates of –5.3 and –6.9 ºC km^{-1}, respectively, averaged over WY 2008-10 in the American and WY 2003-05 in the Yosemite area. As clouds approach the mountain surface during storms (Marks et al. 2013), the atmospheric melting layer is expected to be related to the thickness of the ground rain-snow-transition zone. The atmospheric-melting-layer thickness was ~500 m from bright-band radar (White et al. 2002), and ground-transition-zone thickness was ~500 m using T_{air} thresholds of 0 and 3 °C (Lundquist et al. 2008), with the melting-layer thickness changes depending on humidity, wind, and snow particles (Mizukami et al. 2013). Compared to their typical values, the thickness of the transition zone from this study is narrower, suggesting that the T_{wet} threshold range between temperatures of all snow and all rain could be wider. For example, if doubling the T_{wet} threshold range by setting all snow below –0.5 °C and all rain above 1.5 °C, the thickness of the transition zone would be ~360±90 m, which is closer to the typical melting-layer thickness.

4.2 Difference between rain-snow-transition elevation and atmospheric snow level

The transition elevation estimated from the dense ground-based sensor networks using T_{wet} is generally consistent with snow accumulation and ablation from these spatially distributed nodes (Figures 6, 7, and 8). The transition elevation from the network in the upper elevations of the basins was compared to the atmospheric snow level from the FMCW radars, which are located at lower elevations. While they are defined and measured differently, both are used to estimate precipitation phase in mountain basins. Accordingly, we found reasonable agreement between the two (Figure 9). However, the radar data tend to average ~100 m higher than the on-the-ground transition elevation based on T_{wet} = 0.5 °C (Figure 9) and ~270 m higher than the snow-depth-derived transition elevation (Table 2 and Figure 6). This is consistent with previous findings that freezing level and radar snow level experience lowering on the windward slopes of mountains (Medina et al. 2005; Lundquist et al. 2008; Minder et al. 2011). For this study, the two FMCW radars are strategically placed in lower elevations of the basins to measure snow levels above their elevations throughout the basin. The horizontal distance of ~50 km from radars to the upper wireless-sensor networks on the windward slopes is large enough to show snow-level lowering. As a reference, modeling results showed that the freezing level had a drop of ~400 m over 40 km from the Alta radar profiler to the mountainside of the American basin during a storm (Minder and Kingsmill 2013). Overall, the best-fit slopes are larger than 1.0 for both the American and Feather (Figure 9), showing radar level to be generally higher than on-the-ground transition elevation. This suggests that the snow-level lowering should be accounted for even using radar data at foothills or lower elevations of the basin, due to the colder airmass temperature over short distances caused by adiabatic and latent cooling during the orographic lifting (Minder et al. 2011; Minder and Kingsmill 2013).

Besides the overall tendency of higher radar snow level than ground-transition elevation, Figure 9 also shows that a portion of transition elevation based on T_{wet} = 0.5 °C is higher than the radar snow level. This is partially due to the uncertainties in the T_{wet} regressions (Figure 12b) and outliers in the radar-snow-level data (e.g. Figure 8a and as mentioned by Minder and Kingsmill (2013)). In addition, one possible reason is the temperature difference between ground and atmospheric air, as solar radiation heats the ground but not atmospheric air during storm events (Lundquist et al. 2008). As Figure 15a shows, the differences between transition elevation and radar snow level show a clear diurnal pattern for the American. Radar snow level was generally 140-m higher than transition elevation during nighttime hours (18-06 Pacific Standard Time (PST)), while only 30-m higher during the daylight hours (06-18 PST). Particularly, the radar snow level tended to be lower than the ground-transition elevation during the 09-15 PST. This can be explained by the positive net radiation during daylight hours warming ground air, thus the snow-level-lowering effect (more positive difference in Figure 15a) is compensated. In contrast, the negative net radiation during nighttime hours cools the ground air, and the snow-level-lowering effect tends to be more pronounced. Therefore, the daily cycle of rising and falling ground temperatures caused by net radiation also affects the difference between ground rain-snow-transition elevation and atmospheric snow level.

The diurnal pattern of difference between transition elevation and radar snow level was not found in the more topographically complex Feather (Figure 15b), where 2 of the 4 sensor clusters were located in the eastern, rain-shadow areas blocked by ridges (KTL and GRZ, Figure 2). The two clusters (HMB and BKL) in the western windward ridge benefit from enhanced precipitation caused by orographic lifting. After

condensation in the first ridge, the air loses the majority of water vapor, and descends and expands down the leeward side to the valleys with adiabatic warming (Freeman 2011). Consequently, KTL and GRZ usually show less precipitation (Malek et al. 2019), even though they are at higher elevations. This can be partially indicated by higher relative humidity during WY 2018 snowfalls, where HMB and BKL had values of 97.9 and 98.1%, respectively, versus 96.5 and 95.5% for the KTL and GRZ, respectively. While the horizontal distance between the two clusters in the western windward ridge and other two in rain-shadow areas is large ~50 km, the measured T_{air} still decreases with increasing elevation (0.95, –0.63, –0.69, and –1.45 °C for BKL, HMB, GRZ, and KTL, respectively), supporting the regression of T_{wet} to estimate the ground-transition elevation.

An uncertainty in estimating transition elevation is the spatially inhomogeneous meteorological conditions across both river basins, which could lead to spatially varying rain-snow-transition elevations. While non-uniform transition elevations are challenging to capture by basin-scale wireless-sensor networks, and more so by the radars (Mizukami et al. 2013), they may be represented by high-resolution numerical models. In addition to that, since the Feather is a large basin with more-complex terrain, either the snow level detected by radar at the foothill of the first western windward ridge or the ground-transition elevation estimated from the 4 sensor clusters may not well represent the transition elevation in the rain-shadow areas.

By using the T_{wet}-based method (Wang et al. 2019; Cleave et al. 2019; Tamang et al. 2020) and thresholds selected using on-the-ground snow accumulation and ablation (Figure 5 and Table 2), results from wireless-sensor networks show that the atmospheric-radar snow level tends to be higher than the rain-snow-transition elevation. This is more apparent when the radar snow level is above 2000 m (Figure 9), indicating that particular attention should be given for relevant hydrologic forecasting during high-snow-level storms, such as atmospheric rivers carrying significant water vapor and leading to heavy precipitation. As shown in Figure 16, the event-averaged difference between ground rain-snow-transition elevation and atmospheric snow level is positively correlated to T_{air} (r = 0.33 for the American and 0.54 for the Feather), as well as to mean IVT intensities (not shown, r = 0.45 for the American and 0.56 for the Feather). For the American, the difference during atmospheric-river-related events was 90-m larger than during non-atmospheric-river events (p = 0.06). Similarly, the difference during atmospheric-river-related events tended to be 95-m larger in the Feather (p = 0.27) than during other events. Taken together, the snow-level lowering is more significant (~ 90-m larger) during atmospheric-river-related events with warmer temperature and greater water vapor, than during non-atmospheric-river events. With warmer temperatures, snow-level lowering attributed to adiabatic cooling of rising air increases, as suggested by semi-idealized modeling (Minder et al. 2011). Also, the large water-vapor flux and high precipitation rate during atmospheric-river-related events may enhance the latent cooling effect from meting precipitation and enlarge frozen-hydrometeor melting distance, which in turn contributes to the snow-level lowering during orographic lifting.

4.3 Comparison between the two basins

For the two basins, the transition elevation often ranges over 1400-2200 m, which covers 39% (1860 km^2) of the American but 70% (6600 km^2) of the Feather (Figure 11). The Feather also has a wider thickness of the transition zone, compared to the American (Figure 12c). The proportion of rainfall area in the Feather varies more than in the American (Figures 14a and 14e). Taken together, these point to the Feather being more vulnerable to rising rain-snow transitions than the American, with climate warming potentially resulting in more rain-on-snow events from projections of more-intense atmospheric-river events (Gao et al. 2015; Goldenson et al. 2018). Uncertainty in the rain-snow-transition elevation also has much greater implications for runoff in the Feather, as a 0.5 °C or 100-m uncertainty in the rain-snow-transition elevation corresponds to about 890 km^2, versus only 220 km^2 in the American, at 1800-m elevation. Spatially distributed, on-the-ground data can reduce the uncertainty inherent in a single basin-wide value.

The American tends to exhibit a 100-m higher on-the-ground rain-snow-transition elevation than does the Feather (Figure 10a). Similarly, the radar results also show a higher snow level in the American (Figure 10b). This is caused by warmer mean T_{air} of –0.8 °C in the American than T_{air} of –1.5 °C in the Feather during snowfalls in WY 2017 winter storms, as the Feather has a 1° higher latitude compared to the American. With the warmer temperature of 0.7 °C and a lapse rate of –5 ºC km^{-1}, we expect a 140-m higher rain-snow-transition elevation in the American. The observed difference of on-the-ground transition elevation between two basins (Figure 10) is consistent with the fact that radar snow level decreases with increasing latitude due to regional temperature gradient with colder air in the north (Lundquist et al. 2008; Henn et al. 2020).

4.4 Potential of estimating rain-snow-transition elevation using T_{wet}

By incorporating humidity information, the ground T_{wet} reliably estimated the rain-snow-transition elevation in both the American and Feather, as demonstrated by the consistency with ground-measured snow accumulation and ablation during precipitation events (e.g. Figures 6a, 7, and 8) and the agreement with the atmospheric snow level from radar (Figure 9). Since T_{dew} also incorporates humidity information, it was used to estimate transition elevation by some studies (e.g. Marks et al. 2013; Zhang et al. 2017a). Compared to transition elevation using T_{wet} = 0.5 °C (Figure S2), the elevation of T_{dew} = 0.5 °C was 35-m lower and that of T_{dew} = 0 °C was 50-m higher. This indicates an appropriate T_{dew} threshold may be able to represent similar results based on T_{wet} = 0.5 °C if using the ground data for which evaporation cooling of falling hydrometeors is limited.

Results demonstrate that T_{wet} has a strong linear relationship with elevation across the entire basin during snowfall periods (mean r^2 = 0.84 for the American and 0.87 for the Feather), and a relatively weaker relationship for other times during winter storms (mean r^2 = 0.75 for the American and 0.81 for the Feather). During wintertime snowfall periods, relative humidity is high in the basin and T_{air} declines systematically with elevation, resulting in a lower T_{wet} at higher elevations. More than 66% of the time the T_{wet} lapse rate falls within one standard deviation of the mean ~ –5 ºC km^{-1} (Figure 12c), which may be used to estimate the transition elevation if T_{wet} measurements are limited. Therefore, a strategically placed sensor network with measurements of T_{air} and relative humidity across a basin can provide estimates of the transition elevation and zone with relatively simple, robust measurements and sensors.

The T_{wet}-based method to estimate rain-snow-transition elevation using the wireless-sensor networks has the potential for near-real-time applications. Ground measurements complement information on the radar snow level, and provide spatially distributed ground-truth calibration. The sensor networks also provide important sub-basin information on precipitation patterns in complex topography (Zhang et al., 2017a), which is not captured by radar or operational snow and rain measurement sites. Modeling results showed runoff tripled in three river basins in northern California owing to rising of the transition elevation by 600 m during a storm (White et al. 2002). Taking different transition-elevation estimates on February 8, 2014 in the American River basin as an example (Figure S3), a 460 m higher transition elevation from radar suggested 5.0×10^6 m^3 more (8.9%) potential runoff, and a 120 m lower transition elevation from T_{wet} indicated 2.2×10^6 m^3 less (4.0%) potential runoff, comparing to that from on-the-ground snow-depth-derived transition elevation. Another example in the Feather River basin (Figure S4) showed that a 200-m higher transition elevation could result in 14.8×10^6 m^3 more (34%) potential runoff for one day during an atmospheric-river event. Sumargo et al. (2020) reported that the uncertainty of runoff volume corresponding to a 350-m freezing-level forecast error could be up to half of the Lake Oroville reservoir's flood control storage. These results highlight the importance of accurate rain-snow-transition elevation estimates in mountain basins.

This work is a proof of concept and leaves important questions open for further investigation. Results suggest that the optimum number of sensor clusters, while somewhat basin dependent, is probably somewhere between the four in the Feather and the 13 in the American. Further investigations could address how additional data in the Feather could provide important sub-basin information, and if fewer clusters in the American could provide comparable performance. Also, it should be recognized that this work was done with research networks, which have not been hardened for operational use. The American clusters represent a research investment of over $2 million, and we project that a hardened, reliable operational system would have a similar cost. Annual maintenance for an operational wireless-sensor system may be similar to that for the research network, consisting of annual to semi-annual visits to replace selected sensors, make repairs for any physical damage, and make operational adjustments. This research system is aimed toward operational application for near-real-time rain-snow-transition elevation. At this point, a part of hourly data from the wireless sensor networks is transmitted to CDEC central data hub and displayed in real time (e.g. http://cdec.water.ca.gov/dynamicapp/staMeta?station_id=BTP). Besides that, during the initial research period the wireless-sensor data in the Feather River basin were transmitted to an InfluxDB database and visualized using a Grafana web frontend in real time (Malek et al., 2017, 2019). In general, the data can be telemetered via cellular networks or the Geostationary Operational Environmental Satellite (GOES) depending on location. For the potential application of near-real-time transition elevation, the 15-min wireless sensor data will be first stored in a database and processed for quality assurance and quality control (QAQC) using automatic scripts based on our previous algorithms (Zhang et al. 2017a; Bales et al. 2018; Avanzi et al. 2020; Bales et al. 2020). Then, the data will be averaged to an hourly resolution

for real-time visualization and decision support, and to a daily resolution for planning and evaluation studies. Algorithms based on the T_{wet} and ground snow-depth changes proposed in this study will be applied to estimate the rain-snow-transition elevation, which will be archived in a database and displayed through a publicly accessible dashboard. Furthermore, it is desired to incorporate our data and products into the current operational CDEC system, as the sensor networks pivot from research to operational status. Note that our research system provides a broader suite of measurements and can meet greater data and decision-making needs than described here (Zhang et al., 2017a,b). For example, data from this research system are useful in multiple decision-making contexts, beyond reservoir operations during and after storm events. Other uses include water-supply allocations, drought planning, and watershed management. A more-economical operation can be achieved by spreading costs over multiple public agencies and private stakeholders.

5 Conclusions

This study confirms that strategically placed, spatially distributed on-the-ground continuous observations provide two consistent, complementary methods to detect the rain-snow-transition elevation in mountain basins, and can provide important value-added information not currently available in operational systems. Using hourly temperature, humidity, and snow-depth data from two basin-scale wireless-sensor networks, the on-the-ground rain-snow-transition elevation based on spatial patterns of snow accumulation and ablation was used to define thresholds for wet-bulb temperature that could be used to more-broadly define the rain-snow-transition zone. Analysis of data during 76 winter storms for WY 2014-18 in the American and Feather River basins of California's Sierra Nevada showed a wet-bulb temperature threshold of 0.5 °C to give the best consistency with increases (snowfall) or decreases (rainfall) in snow depth. For many events, dew-point temperature also provides an index to accurately define the rain-snow transition. Estimates of the rain-snow-transition elevation using wet-bulb temperature showed good agreement (r = 0.85) with radar-detected atmospheric snow levels in the two basins. However, the transition elevation from the ground networks was about 100 m higher than the radar snow level, which was observed at a lower elevation.

For both basins, the transition elevation is most often in the 1400-2200 m elevation range (probability >53%) and 66% of the time the lapse rate of T_{wet} was about –5 ^{o}C km^{-1}. Owing to more-complex terrain and fewer sensor-clusters in the Feather, transition-elevation estimates were associated with higher uncertainties in the Feather than were the American. Overall, the Feather is more vulnerable than the American to a rising rain-snow transition and to uncertainty in the transition elevation due to its topographic characteristics, i.e. substantially larger area in the transition zone, compared to the American. Atmospheric-river events had a 155-m higher rain-snow-transition than non-atmospheric-river events. Thus, larger proportions of rainfall area were shown during atmospheric-river events. Atmospheric-river events had significantly larger potential runoff due to more-intense precipitation caused by larger IVT intensities. Besides that, the difference between atmospheric snow level and ground transition elevation during atmospheric-river events was 90-m larger than for non-atmospheric-river events, showing enhanced snow level-lowering during orographic lifting of warmer air mass with greater water vapor.

This method demonstrated in this study can be further extended to provide near-real-time information on the on-the-ground rain versus snow area in mountain basins, as complementary to atmospheric snow level from radar or freezing level from numerical models. Applications of basin-scale wireless-sensor networks provide a pathway to advance our knowledge of precipitation-phase partitioning and other decision-relevant hydrologic attributes in mixed rain-snow regions.

Acknowledgments

This research was supported by the UC Water Security and Sustainability Research Initiative grant No. 13941, Electric Program Investment Charge program grant EPC-14-067 from the California Energy Commission, the NSF Southern Sierra Critical Zone Observatory (EAR-1331939), and the NSF Major Research Instrumentation Grant (EAR-1126887). We thank the California Department of Water Resources and Pacific Gas & Electric for their support. Thank you to Danny Marks for the discussion of wet-bulb temperature in the iSnobal model and to three anonymous reviewers for important, constructive comments.

Supplemental Material

The Supplemental Material for this article can be found below.

References

Avanzi, F., Z. Zheng, A. Coogan, R. Rice, R. Akella, and M. H. Conklin, 2020: Gap-filling snow-depth time-series with Kalman Filtering-Smoothing and Expectation Maximization: Proof of concept using spatially dense wireless-sensor-network data. *Cold Reg. Sci. Technol.*, 175, 103066, https://doi.org/10.1016/j.coldregions.2020.103066.

Bales, R. C., N. P. Molotch, T. H. Painter, M. D. Dettinger, R. Rice, and J. Dozier, 2006: Mountain hydrology of the

western United States. *Water Resour. Res.*, 42, 1–13, https://doi.org/10.1029/2005WR004387.

——, E. Stacy, M. Safeeq, X. Meng, M. Meadows, C. Oroza, M. Conklin, S. Glaser, and J. Wagenbrenner, 2018: Spatially distributed water-balance and meteorological data from the rain-snow transition, southern Sierra Nevada, California. *Earth Syst. Sci. Data Discuss.*, 10, 1795–1805, https://doi.org/10.5194/essd-10-1795-2018.

——, G. Cui, R. Rice, X. Meng, Z. Zhang, P. Hartsough, S. Glaser, and M. Conklin, 2020: Snow depth, air temperature, humidity, soil moisture and temperature, and solar radiation data from the basin-scale wireless-sensor network in American River Hydrologic Observatory (ARHO). *UC Merced, Dataset*, https://doi.org/10.6071/M39Q2V.

Behrangi, A., X. Yin, S. Rajagopal, D. Stampoulis, and H. Ye, 2018: On distinguishing snowfall from rainfall using near-surface atmospheric information: Comparative analysis, uncertainties and hydrologic importance. *Q. J. R. Meteorol. Soc.*, 144, 89–102, https://doi.org/10.1002/qj.3240.

Cannon, F., F. M. Ralph, A. M. Wilson, and D. P. Lettenmaier, 2017: GPM satellite radar measurements of precipitation and freezing level in Atmospheric Rivers: Comparison with ground-based radars and reanalyses. *J. Geophys. Res. Atmos.*, 122, 747–764, https://doi.org/10.1002/2017JD027355.

Cleave, D. Van, R. Graham, D. Myrick, and M. Nordquist, 2019: *Snow Level in the NWS Western Region : Definition and Calculation Methodology*. 1–5 pp. [Available online at https://www.weather.gov/media/wrh/online_publications/TAs/TA1901.pdf].

Daly, C., M. Halbleib, J. I. Smith, W. P. Gibson, M. K. Doggett, G. H. Taylor, J. Curtis, and P. P. Pasteris, 2008: Physiographically sensitive mapping of climatological temperature and precipitation across the conterminous United States. *Int. J. Climatol.*, 28, 2031–2064, https://doi.org/10.1002/joc.1688.

Demaria, E. M. C., F. Dominguez, H. Hu, G. von Glinski, M. Robles, J. Skindlov, and J. Walter, 2017: Observed hydrologic impacts of landfalling atmospheric rivers in the Salt and Verde river basins of Arizona, United States. *Water Resour. Res.*, 53, 10025–10042, https://doi.org/10.1002/2017WR020778.

Dettinger, M. D., F. M. Ralph, T. Das, P. J. Neiman, and D. R. Cayan, 2011: Atmospheric rivers, floods and the water resources of California. *Water*, 3, 445–478, https://doi.org/10.3390/w3020445.

Ding, B., K. Yang, J. Qin, L. Wang, Y. Chen, and X. He, 2014: The dependence of precipitation types on surface elevation and meteorological conditions and its parameterization. *J. Hydrol.*, 513, 154–163, https://doi.org/10.1016/j.jhydrol.2014.03.038.

Feld, S. I., N. C. Cristea, and J. D. Lundquist, 2013: Representing atmospheric moisture content along mountain slopes: Examination using distributed sensors in the Sierra Nevada, California. *Water Resour. Res.*, 49, 4424–4441, https://doi.org/10.1002/wrcr.20318.

Freeman, G. J., 2011: Climate change and the changing water balance for California's North Fork River. *Proceedings of the 79th Annual Western Snow Conference*, Stateline, NV, Western Snow Conference, 71–82.

Gao, Y., J. Lu, L. R. Leung, Q. Yang, S. Hagos, and Y. Qian, 2015: Dynamical and thermodynamical modulations on future changes of landfalling atmospheric rivers over western North America. *Geophys. Res. Lett.*, 42, 7179–7186, https://doi.org/10.1002/2015GL065435.

Gelaro, R., and Coauthors, 2017: The modern-era retrospective analysis for research and applications, version 2 (MERRA-2). *J. Clim.*, 30, 5419–5454, https://doi.org/10.1175/JCLI-D-16-0758.1.

Goldenson, N., L. R. R. Leung, C. M. M. Bitz, and E. Blanchard-Wrigglesworth, 2018: Influence of Atmospheric Rivers on mountain snowpack in the Western United States. *J. Clim.*, 31, 9921–9940, https://doi.org/10.1175/JCLI-D-18-0268.1.

Harpold, A. A., and Coauthors, 2017: Rain or snow: hydrologic processes, observations, prediction, and research needs. *Hydrol. Earth Syst. Sci.*, 21, 1–22, https://doi.org/10.5194/hess-21-1-2017.

Hatchett, B., B. Daudert, C. Garner, N. Oakley, A. Putnam, and A. White, 2017: Winter snow level rise in the northern Sierra Nevada from 2008 to 2017. *Water*, 9, 899, https://doi.org/10.3390/w9110899.

Henn, B., R. Weihs, A. C. Martin, F. M. Ralph, and T. Osborne, 2020: Skill of rain-snow level forecasts for landfalling atmospheric rivers: A multi-model model assessment using California's network of vertically profiling radars. *J. Hydrometeorol.*, 21, 751–771, https://doi.org/10.1175/jhm-d-18-0212.1.

Huning, L. S., B. Guan, D. E. Waliser, and D. P. Lettenmaier, 2019: Sensitivity of seasonal snowfall attribution to Atmospheric Rivers and their reanalysis-based detection. *Geophys. Res. Lett.*, 46, 794–803, https://doi.org/10.1029/2018GL080783.

Jennings, K. S., and N. P. Molotch, 2019: The sensitivity of modeled snow accumulation and melt to precipitation phase methods across a climatic gradient. *Hydrol. Earth Syst. Sci. Discuss.*, 23, 1–33, https://doi.org/10.5194/hess-2019-82.

Jennings, K. S., T. S. Winchell, B. Livneh, and N. P. Molotch, 2018: Spatial variation of the rain-snow temperature threshold across the Northern Hemisphere. *Nat. Commun.*, 9, 1–9, https://doi.org/10.1038/s41467-018-03629-7.

Johnston, P. E., D. A. Carter, J. R. Jordan, and A. B. White, 2009: A new snow-level detection radar. *34th Conf. Radar Meteorol.*.

Johnston, P. E., J. R. Jordan, A. B. White, D. A. Carter, D. M. Costa, and T. E. Ayers, 2017: The NOAA FM-CW snow-level radar. *J. Atmos. Ocean. Technol.*, 34, 249–267, https://doi.org/10.1175/JTECH-D-16-0063.1.

Koczot, K. M., A. E. Jeton, B. J. McGurk, and M. D. Dettinger, 2004: Precipitation-runoff processes in the Feather River Basin, northeastern California, with prospects for streamflow predictability, water years 1971–97. U.S. Geological Survey Scientific Investigations

Report 2004-5202. 82 pp. [Available online at https://pubs.usgs.gov/sir/2004/5202/sir2004-5202.pdf].

Lawrence, M. G., 2005: The relationship between relative humidity and the dewpoint temperature in moist air: A simple conversion and applications. *Bull. Am. Meteorol. Soc.*, 86, 225–234, https://doi.org/10.1175/BAMS-86-2-225.

Lettenmaier, D. P., 2019: Atmospheric river-induced precipitation and snowpack during the western United States cold season. *J. Hydrometeorol.*, 20, 613–630, https://doi.org/10.1175/JHM-D-18-0228.1.

Lundquist, J. D., P. J. Neiman, B. Martner, A. B. White, D. J. Gottas, and F. M. Ralph, 2008: Rain versus snow in the Sierra Nevada, California: Comparing Doppler profiling radar and surface observations of melting level. *J. Hydrometeorol.*, 9, 194–211, https://doi.org/10.1175/2007JHM853.1.

Malek, S. A., F. Avanzi, K. Brun-Laguna, T. Maurer, C. A. Oroza, P. C. Hartsough, T. Watteyne, and S. D. Glaser, 2017: Real-time alpine measurement system using wireless sensor networks. *Sensors (Switzerland)*, 17, 1–30, https://doi.org/10.3390/s17112583.

——, S. D. Glaser, and R. C. Bales, 2019: Wireless Sensor Networks for improved snow water equivalent and runoff estimates. *IEEE Access*, 7, 18420–18436, https://doi.org/10.1109/ACCESS.2019.2895397.

Marks, D., A. Winstral, M. Reba, J. Pomeroy, and M. Kumar, 2013: An evaluation of methods for determining during-storm precipitation phase and the rain/snow transition elevation at the surface in a mountain basin. *Adv. Water Resour.*, 55, 98–110, https://doi.org/10.1016/j.advwatres.2012.11.012.

Marwitz, J. D., 1983: The kinematics of orographic airflow during Sierra storms. *J. Atmos. Sci.*, 40, 1218–1227, https://doi.org/10.1175/1520-0469(1983)040<1218:TKOOAD>2.0.CO;2.

——, 1987: Deep orographic storms over the Sierra Nevada. Part I: thermodynamic and kinematic structure. *J. Atmos. Sci.*, 44, 159–173, https://doi.org/10.1175/1520-0469(1987)044<0159:DOSOTS>2.0.CO;2.

Matrosov, S. Y., R. Cifelli, A. White, and T. Coleman, 2017: Snow-level estimates using operational polarimetric weather radar measurements. *J. Hydrometeorol.*, 18, 1009–1019, https://doi.org/10.1175/JHM-D-16-0238.1.

Medina, S., B. F. Smull, R. A. Houze, and M. Steiner, 2005: Cross-barrier flow during orographic precipitation events: Results from MAP and IMPROVE. *J. Atmos. Sci.*, 62, 3580–3598, https://doi.org/10.1175/JAS3554.1.

Minder, J. R., and D. E. Kingsmill, 2013: Mesoscale variations of the atmospheric snow line over the northern Sierra Nevada: Multiyear statistics, case study, and mechanisms. *J. Atmos. Sci.*, 70, 916–938, https://doi.org/10.1175/JAS-D-12-0194.1.

——, D. R. Durran, and G. H. Roe, 2011: Mesoscale controls on the mountainside snow line. *J. Atmos. Sci.*, 68, 2107–2127, https://doi.org/10.1175/JAS-D-10-05006.1.

Mizukami, N., V. Koren, M. Smith, D. Kingsmill, Z. Zhang, B. Cosgrove, and Z. Cui, 2013: The impact of precipitation type discrimination on hydrologic simulation: Rain–snow partitioning derived from HMT-West radar-detected brightband height versus surface temperature data. *J. Hydrometeorol.*, 14, 1139–1158, https://doi.org/10.1175/JHM-D-12-035.1.

Musselman, K. N., F. Lehner, K. Ikeda, M. P. Clark, A. F. Prein, C. Liu, M. Barlage, and R. Rasmussen, 2018: Projected increases and shifts in rain-on-snow flood risk over western North America. *Nat. Clim. Chang.*, 8, 808–812, https://doi.org/10.1038/s41558-018-0236-4.

Neiman, P. J., F. M. Ralph, G. A. Wick, J. D. Lundquist, and M. D. Dettinger, 2008: Meteorological characteristics and overland precipitation impacts of atmospheric rivers affecting the West Coast of North America based on eight years of SSM/I satellite observations. *J. Hydrometeorol.*, 9, 22–47, https://doi.org/10.1175/2007JHM855.1.

——, L. J. Schick, F. M. Ralph, M. Hughes, and G. A. Wick, 2011: Flooding in western Washington: The connection to atmospheric rivers. *J. Hydrometeorol.*, 12, 1337–1358, https://doi.org/10.1175/2011JHM1358.1.

——, F. M. Ralph, B. J. Moore, M. Hughes, K. M. Mahoney, J. M. Cordeira, and M. D. Dettinger, 2013: The landfall and inland penetration of a flood-producing atmospheric river in Arizona. Part I: Observed synoptic-scale, orographic, and hydrometeorological characteristics. *J. Hydrometeorol.*, 14, 460–484, https://doi.org/10.1175/JHM-D-12-0101.1.

Ohara, N., M. L. Kavvas, S. Kure, Z. Chen, S. Jang, and E. Tan, 2011: Physically based estimation of maximum precipitation over American River Watershed, California. *J. Hydrol. Eng.*, 16, 351–361, https://doi.org/10.1061/(ASCE)HE.1943-5584.0000324.

Olsen, A., 2003: *Snow or rain ? - A matter of wet-bulb temperature*. [Available online at https://www.diva-portal.org/smash/get/diva2:968860/FULLTEXT01.pdf].

Ralph, F. M., P. J. Neiman, and G. A. Wick, 2004: Satellite and CALJET aircraft observations of atmospheric rivers over the eastern North Pacific Ocean during the winter of 1997/98. *Mon. Weather Rev.*, 132, 1721–1745, https://doi.org/10.1175/1520-0493(2004)132<1721:SACAOO>2.0.CO;2.

——, M. C. L. D. Dettinger, M. M. Cairns, T. J. Galarneau, and J. Eylander, 2018: Defining “atmospheric river”: How the glossary of meteorology helped resolve a debate. *Bull. Am. Meteorol. Soc.*, 99, 837–839, https://doi.org/10.1175/BAMS-D-17-0157.1.

Ralph, F. M., J. J. Rutz, J. M. Cordeira, M. Dettinger, M. Anderson, D. Reynolds, L. J. Schick, and C. Smallcomb, 2019: A scale to characterize the strength and impacts of atmospheric rivers. *Bull. Am. Meteorol. Soc.*, 100, 269–289, https://doi.org/10.1175/BAMS-D-18-0023.1.

Risley, J., H. Moradkhani, L. Hay, and S. Markstrom, 2011: Statistical comparisons of watershed-scale response to climate change in selected basins across the United States. *Earth Interact.*, 15, 1–26, https://doi.org/10.1175/2010EI364.1.

Sims, E. M., and G. Liu, 2015: A parameterization of the probability of snow–rain transition. *J. Hydrometeorol.*, 16, 1466–1477, https://doi.org/10.1175/JHM-D-14-0211.1.

Sumargo, E., F. Cannon, F. M. Ralph, and B. Henn, 2020: Freezing level forecast error can consume reservoir flood control storage: Potentials for Lake Oroville and New Bullards Bar Reservoirs in California. *Water Resour. Res.*, https://doi.org/10.1029/2020WR027072.

Tamang, S. K., A. M. Ebtehaj, A. F. Prein, and A. J. Heymsfield, 2020: Linking global changes of snowfall and wet-bulb temperature. *J. Clim.*, 33, 39–59, https://doi.org/10.1175/jcli-d-19-0254.1.

Wang, Y., P. Broxton, Y. Fang, A. Behrangi, M. Barlage, X. Zeng, and G. Niu, 2019: A Wet-Bulb Temperature-Based Rain-Snow Partitioning Scheme Improves Snowpack Prediction Over the Drier Western United States. *Geophys. Res. Lett.*, 46, 13825-13835, https://doi.org/10.1029/2019GL085722.

Welch, S. C., B. Kerkez, R. C. Bales, S. D. Glaser, K. Rittger, and R. R. Rice, 2013: Sensor placement strategies for snow water equivalent (SWE) estimation in the American River basin. *Water Resour. Res.*, 49, 891–903, https://doi.org/10.1002/wrcr.20100.

White, A. B., D. J. Gottas, E. T. Strem, F. M. Ralph, and P. J. Neiman, 2002: An automated brightband height detection algorithm for use with Doppler radar spectral moments. *J. Atmos. Ocean. Technol.*, 19, 687–697, https://doi.org/10.1175/1520-0426(2002)019<0687:AABHDA>2.0.CO;2.

——, ——, A. F. Henkel, P. J. Neiman, F. M. Ralph, and S. I. Gutman, 2010: Developing a performance measure for snow-level forecasts. *J. Hydrometeorol.*, 11, 739–753, https://doi.org/10.1175/2009JHM1181.1.

White, A. B., and Coauthors, 2013: A twenty-first-century california observing network for monitoring extreme weather events. *J. Atmos. Ocean. Technol.*, 30, 1585–1603, https://doi.org/10.1175/JTECH-D-12-00217.1.

White, A. B., B. J. Moore, D. J. Gottas, and P. J. Neiman, 2019: Winter storm conditions leading to excessive runoff above California's Oroville Dam during January and February 2017. *Bull. Am. Meteorol. Soc.*, 100, 55–70, https://doi.org/10.1175/BAMS-D-18-0091.1.

Yigzaw, W., F. Hossain, and A. Kalyanapu, 2013: Impact of artificial reservoir size and land use/land cover patterns on probable maximum precipitation and flood: Case of folsom dam on the American river. *J. Hydrol. Eng.*, 18, 1180–1190, https://doi.org/10.1061/(ASCE)HE.1943-5584.0000722.

Zagrodnik, J. P., L. A. McMurdie, and R. A. Houze, 2018: Stratiform precipitation processes in cyclones passing over a coastal mountain range. *J. Atmos. Sci.*, 75, 983–1004, https://doi.org/10.1175/JAS-D-17-0168.1.

Zhang, Z., S. Glaser, R. Bales, M. Conklin, R. Rice, and D. Marks, 2017a: Insights into mountain precipitation and snowpack from a basin-scale wireless-sensor network. *Water Resour. Res.*, 53, 6626–6641, https://doi.org/10.1002/2016WR018825.

Zhang, Z., S. D. Glaser, R. C. Bales, M. Conklin, R. Rice, and D. G. Marks, 2017b: Technical report: The design and evaluation of a basin-scale wireless sensor network for mountain hydrology. *Water Resour. Res.*, 53, 4487–4498, https://doi.org/10.1002/2016WR019619.

Zhong, K., F. Zheng, X. Xu, and C. Qin, 2018: Discriminating the precipitation phase based on different temperature thresholds in the Songhua River Basin, China. *Atmos. Res.*, 205, 48–59, https://doi.org/10.1016/j.atmosres.2018.02.002.

Zhu, Y., and R. E. Newell, 1994: Atmospheric rivers and bombs. *Geophys. Res. Lett.*, 21, 1999–2002, https://doi.org/10.1029/94GL01710.

Table 1. List of wireless sensor clusters in the American and Feather River basins

River basin	Wireless sensor cluster	Abbreviation	Co-located gauge*	Lat, °	Lon, °	Elevation, m
American	Schneiders	SCN		38.745	-120.068	2673
	Echo Peak	ECP		38.851	-120.075	2473
	Mt Lincoln	MTL		39.286	-120.325	2467
	Caples Lake	CAP	CAP	38.711	-120.042	2437
	Alpha	ALP	FRN	38.805	-120.214	2269
	Duncan Peak	DUN		39.152	-120.511	2098
	Van Vleck	VVL		38.943	-120.309	2071
	Dolly Rice	DOR		39.149	-120.371	1983
	Onion Creek	ONN		39.276	-120.358	1891
	Robbs Saddle	RBB		38.913	-120.379	1812
	Talbot Camp	TLC		39.191	-120.377	1739
	Owens Camp	OWC	OWC	38.736	-120.242	1586
	Bear Trap	BTP	BTP	39.093	-120.577	1582
Feather	Kettle Rock	KTL	KTL	40.139	-120.714	2206
	Grizzly Ridge	GRZ	GRZ	39.919	-120.641	2068
	Humbug	HMB	HMB	40.120	-121.375	2008
	Bucks Lake	BKL	BKL	39.855	-121.251	1742

* Co-located precipitation gauge on CDEC

Table 2. Rain-snow-transition elevation from different T_{wet} thresholds and radar snow level, compared to snow-depth-derived transition elevation. RMSD: root mean squared difference, and positive mean difference (or percent difference) indicates the corresponding results are higher than ground snow-depth-derived transition elevation.

	T_{wet}, °C						Radar
	–1	–0.5	0	**0.5**	1	1.5	
RMSD, m	327	251	187	**155**	170	224	372
Mean difference, m	290	200	110	**21**	–69	–159	272
Percent difference	14.1%	9.7%	5.4%	**1.0%**	–3.4%	–7.7%	13.3%

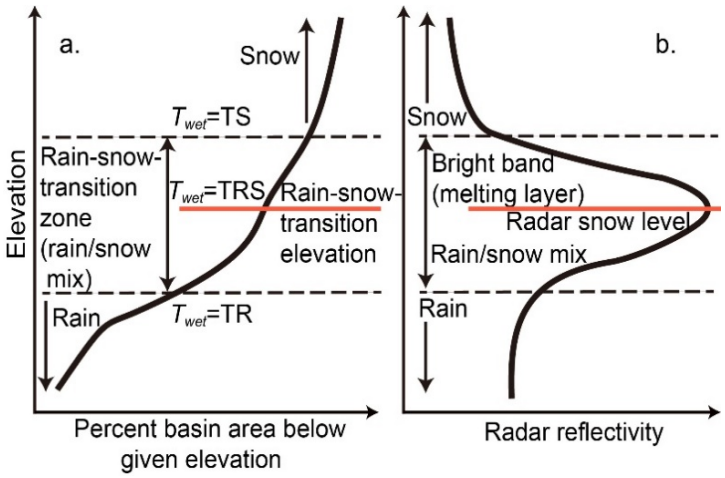

Figure 1. Schematics of (a) the rain-snow-transition elevation (solid red line) and zone (between two black dashed lines) estimated from a wet-bulb temperature (T_{wet}) method. The T_{wet} thresholds for rain, rain-snow transition, and snow are labeled as TR, TRS, and TS, respectively. And (b) the FMCW radar-derived atmospheric snow level (red line) and melting layer based on radar reflectivity in an atmospheric column, modified after Mizukami et al. (2013).

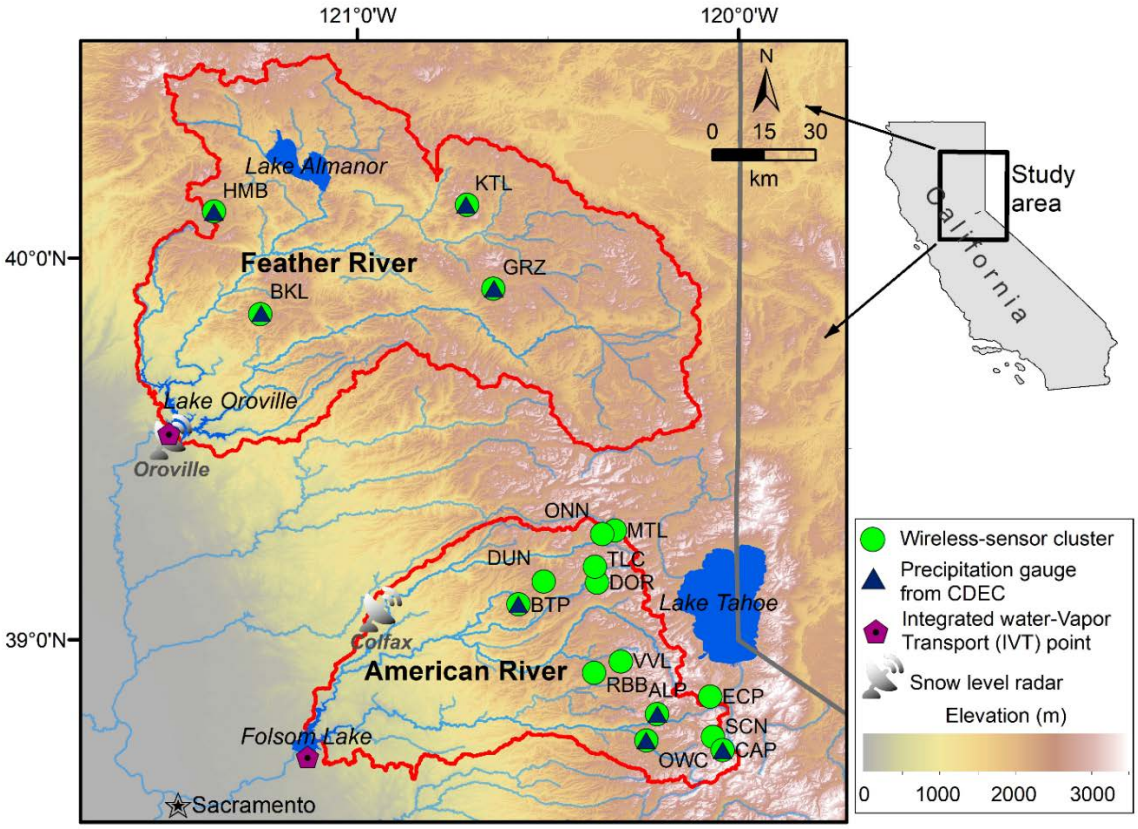

Figure 2. Location of wireless-sensor networks in the American and Feather River basins.

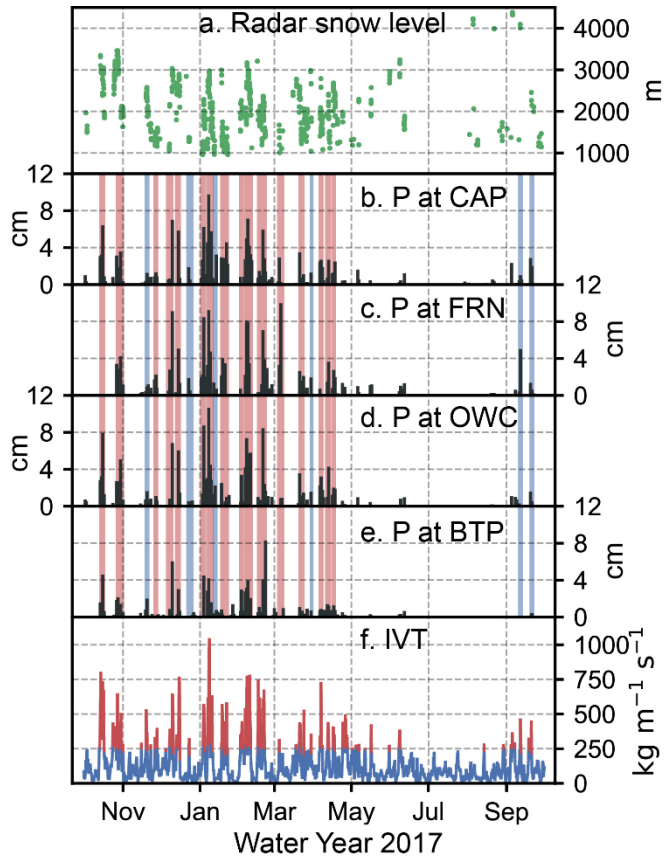

Figure 3. WY 2017 storm events selected using observations in the American River basin. (a) hourly FMCW radar-detected atmospheric snow level at Colfax, (b)-(e) show the precipitation (P, black) measured by precipitation gauges at CAP (2437 m), FRN (2269 m), OWC (1586 m), and BTP (1582 m) sites from CDEC, respectively (Figure 2). Shaded bands indicate selected storm events, red bands for atmospheric-river events and blue bands for non-atmospheric-river events. Panel (f) shows Integrated water-Vapor Transport (IVT) at Folsom Dam, from the MERRA-2 dataset, with intensities larger than a threshold of 250 kg m^{-1} s^{-1} marked as red.

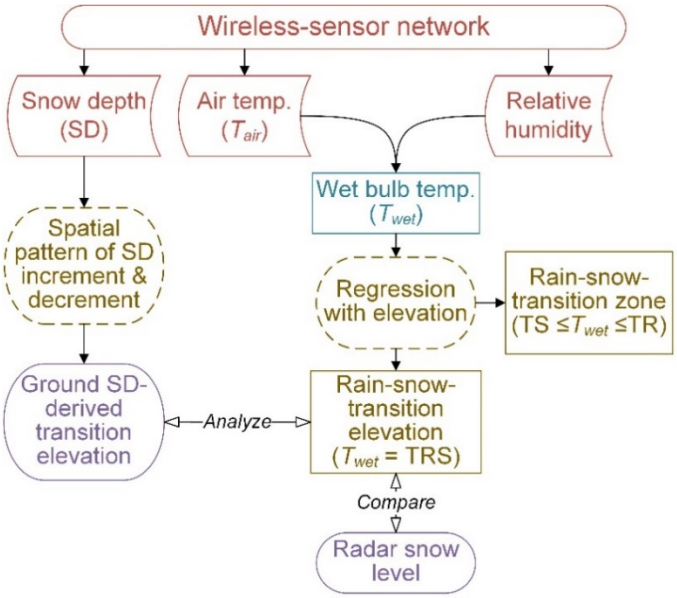

Figure 4. Flowchart of data and method to determine rain-snow-transition elevation and zone. The T_{wet} thresholds for rain, rain-snow transition, and snow are labeled as TR, TRS, and TS, respectively.

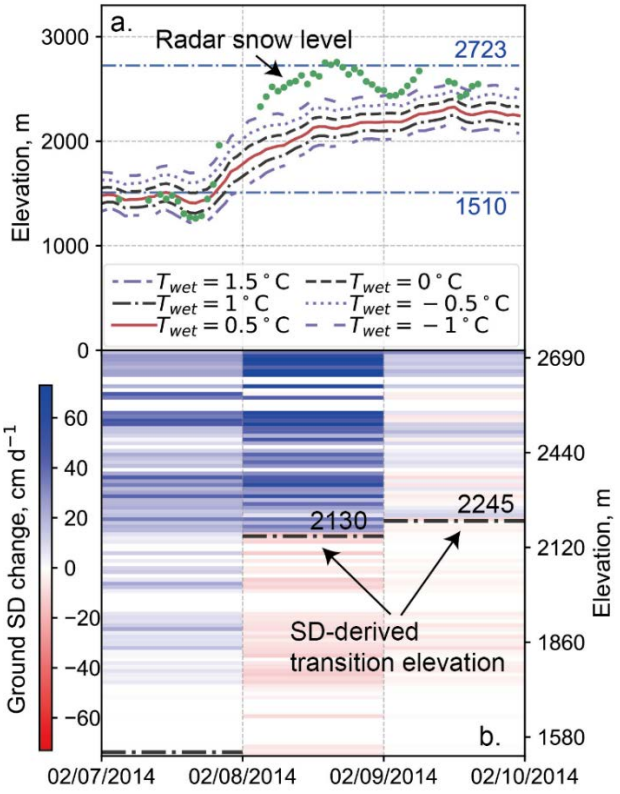

Figure 5. An example of elevation at different T_{wet} thresholds and radar snow level (a) versus ground snow-depth(SD)-derived transition elevation from spatially distributed wireless-sensor nodes in the American River basin (b). Blue lines in (a) denote the elevation range (1510-2723 m) of the wireless-sensor clusters. Each colored line in (b) is daily snow-depth increment (blue) or decrement (red) measured by each sensor node at its elevation.

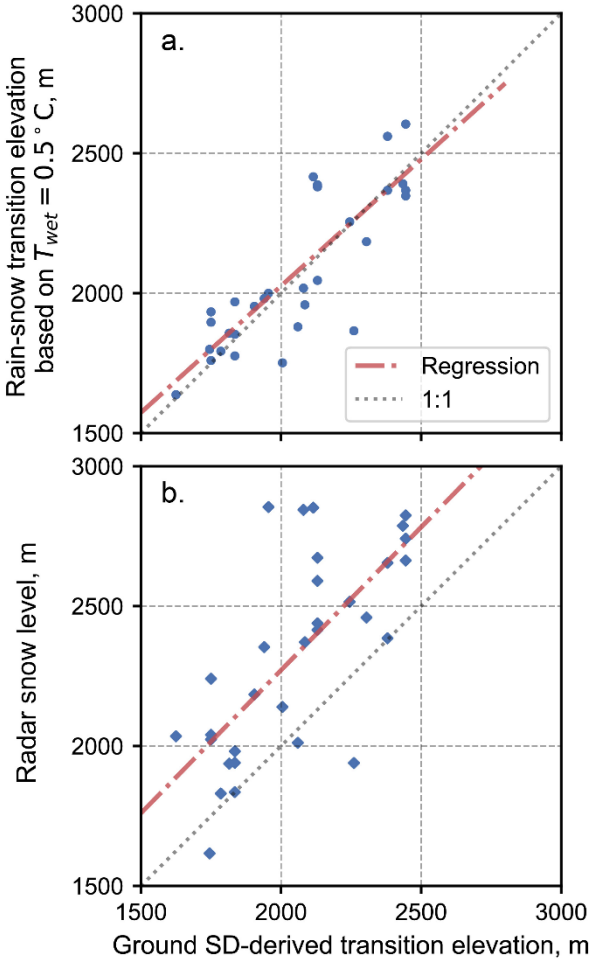

Figure 6. Rain-snow-transition elevation based on T_{wet} = 0.5 °C (a) and radar snow level (b), compared to the ground snow-depth(SD)-derived transition elevation from wireless-sensor nodes in the American River basin, for 31 days in WY 2014-17 when the pattern of snow-depth increment or decrement was confidently differentiated within the elevation range of the sensor nodes.

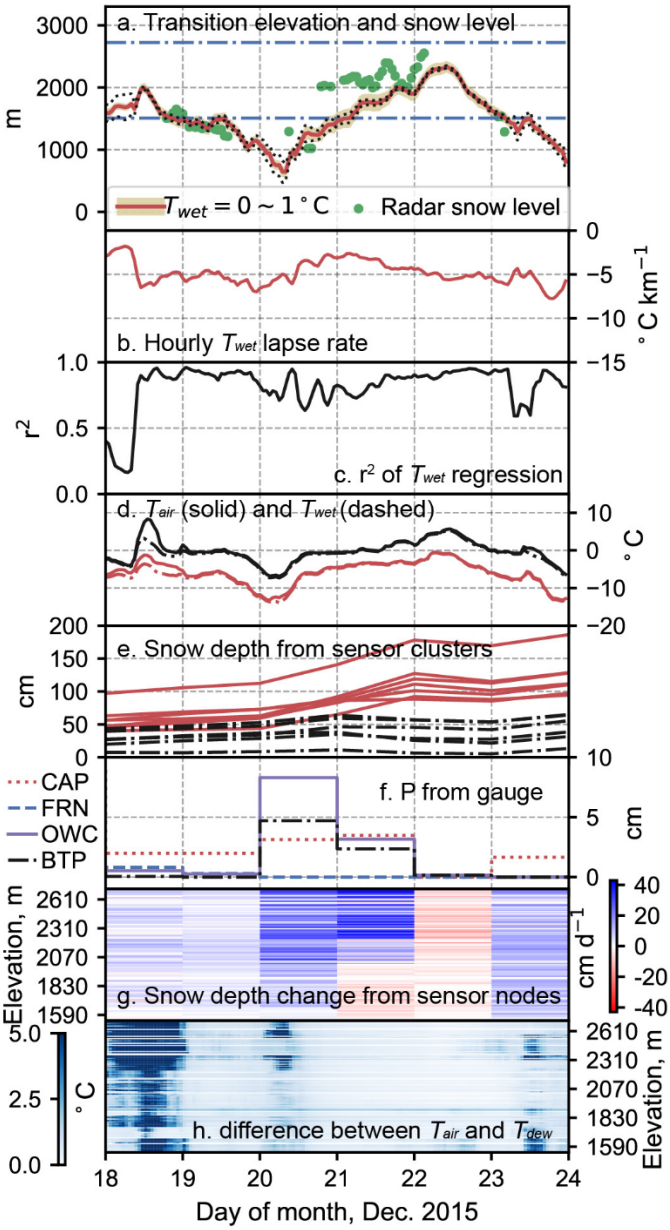

Figure 7. Characteristics of an event in December 2015 in the American River basin: (a) rain-snow-transition zone (shaded area of T_{wet} in range of 0 ~ 1 °C), transition elevation (red line for T_{wet} = 0.5 °C), and snow level from the radar at Colfax (green dot). Black dotted lines are the 95% confidence interval of the regression-derived elevation of T_{wet} = 0.5 °C. Blue lines denote the elevation range (1510-2723 m) of the wireless-sensor clusters; (b) T_{wet} lapse rate from an hourly regression between on-the-ground T_{wet} and their elevations; (c) r^2 of the regression; (d) T_{air} (solid) and T_{wet} (dashed) at the highest (red, 2723 m) and the lowest (black, 1510 m) sensor nodes, (e) daily average snow depth from the sensor clusters, red solid lines denote higher elevation clusters and black dashed lines for lower clusters based on their elevational ranking; (f) daily precipitation (P) from available precipitation gauge stations on CDEC; (g) daily snow-depth change from each sensor node; (h) hourly difference between T_{air} and T_{dew} at each sensor node.

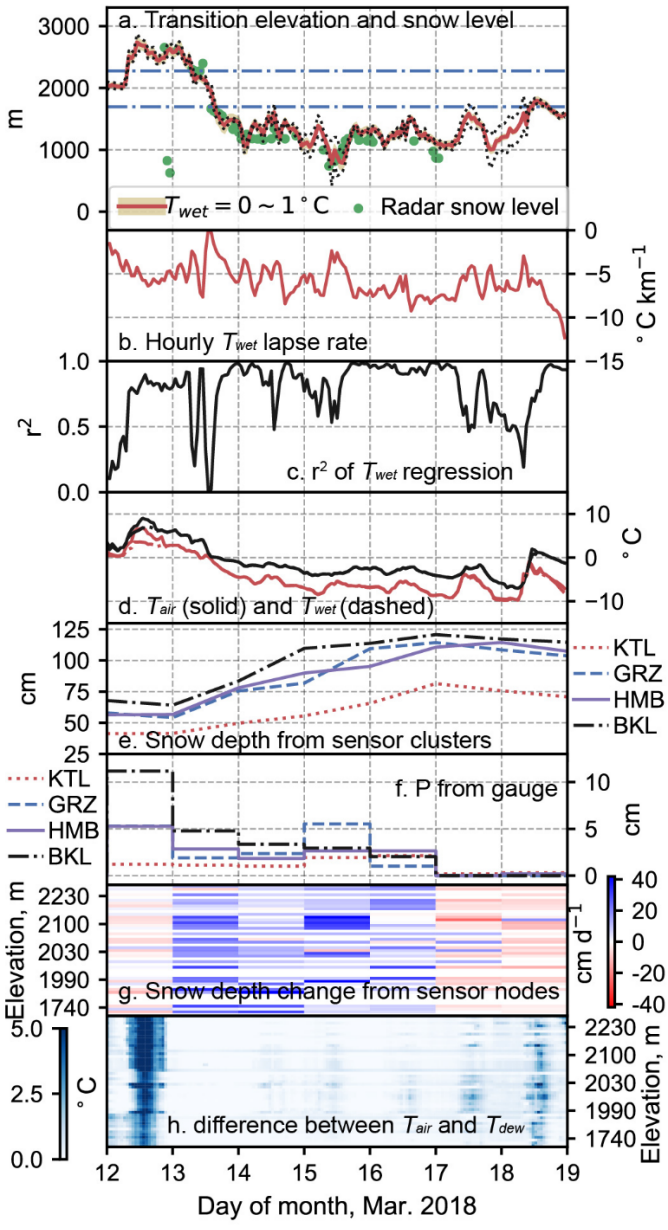

Figure 8. Characteristics of an event in March 2018 in the Feather River basin: (a) rain-snow-transition zone (shaded area of T_{wet} in range of 0 ~ 1 °C), transition elevation (red line for T_{wet} = 0.5 °C), and snow level from radar at Oroville (green dot). Black dotted lines are the 95% confidence interval of the regression-derived elevation of T_{wet} = 0.5 °C. Blue lines denote the elevation range (1697-2277 m) of the sensor clusters; (b) T_{wet} lapse rate from an hourly regression between on-the-ground T_{wet} and their elevations; (c) r^2 of the regression; (d) T_{air} (solid) and T_{wet} (dashed) at the highest (red, 2277 m) and the lowest (black, 1697 m) sensor nodes; (e) daily average snow depth from the sensor clusters; (f) daily precipitation (P) from available precipitation gauge stations on CDEC; (g) daily snow-depth change from each sensor node; (h) hourly difference between T_{air} and T_{dew} at each sensor node.

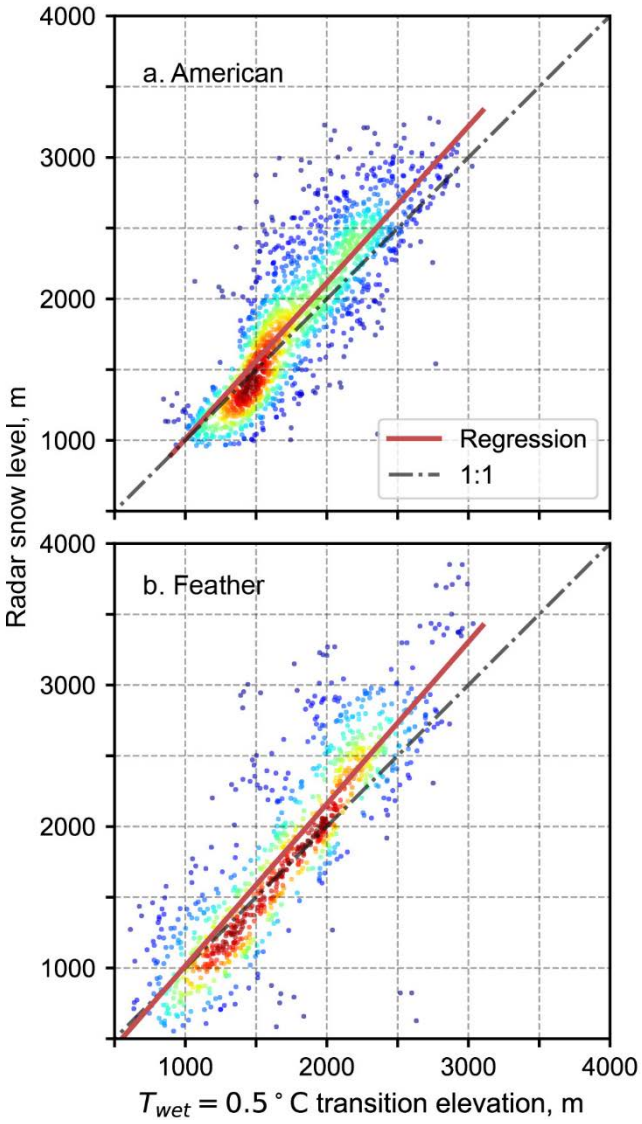

Figure 9. Rain-snow-transition elevation at T_{wet} = 0.5 °C from the wireless-sensor networks versus radar snow level during events in November-April: (a) the American River basin for WY 2014-17 and (b) the Feather River basin for WY 2017-18. Red line is the regression line of the dots colored by point density (red for high density and blue for low density).

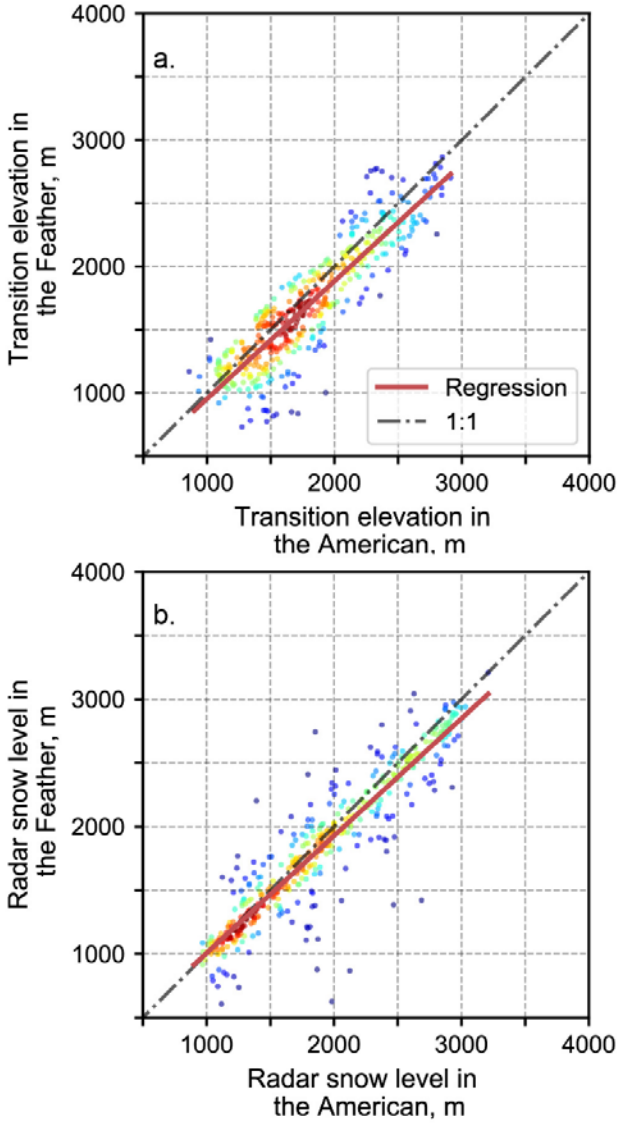

Figure 10. (a) Hourly rain-snow-transition elevation based on T_{wet} = 0.5 °C using the wireless-sensor networks in the American and Feather River basins from November to April in WY 2017 and (b) the same as (a), but for atmospheric snow level from radars. Red line is the regression line of the dots colored by point density (red for high density and blue for low density).

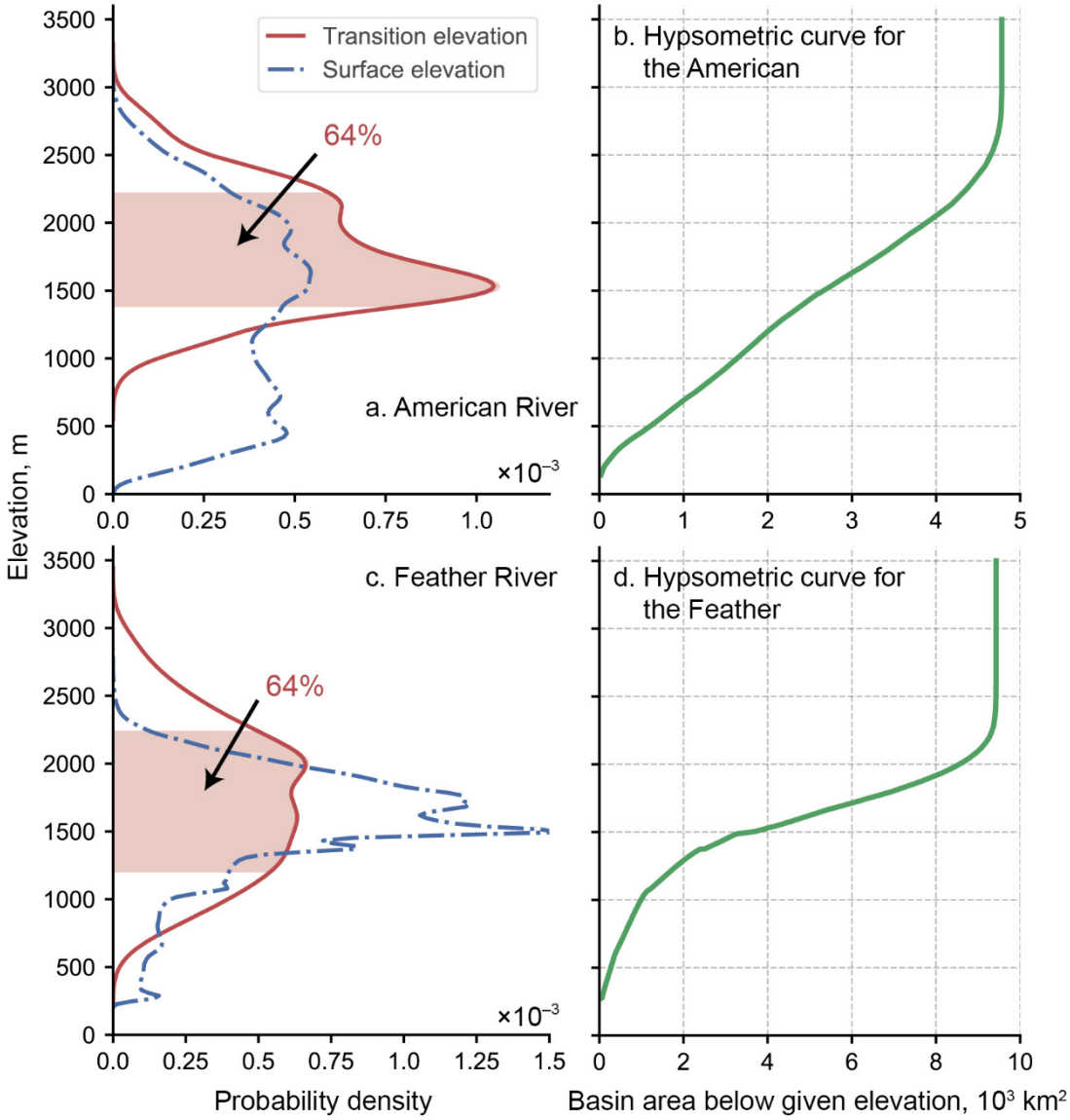

Figure 11. Probability density of rain-snow-transition elevation (red line) from the wireless-sensor networks for (a) the American River basin WY 2014-17 and (c) the Feather River basin WY 2017-18. The blue lines show the probability density function of basin surface elevation. The probabilities of shade bands (areas of mean ± standard deviation) for transition elevation are labeled. (b) and (d) show hypsometric curves for the American and Feather River basins, respectively.

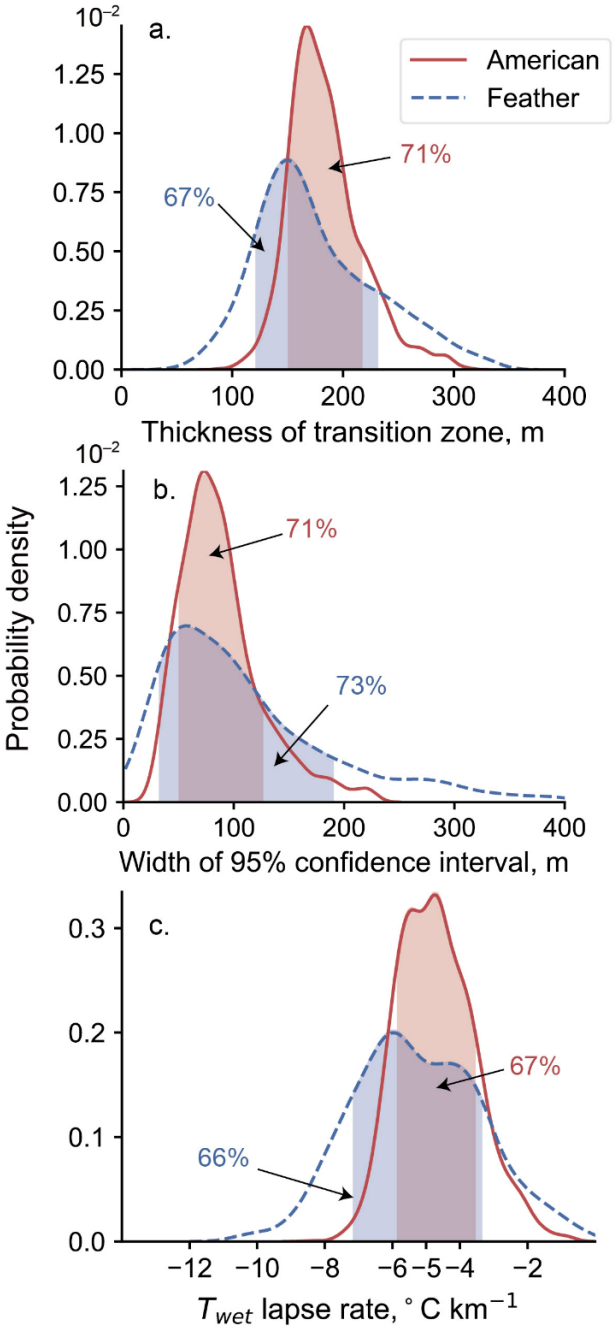

Figure 12. Probability density of (a) thickness of the rain-snow-transition zone (T_{wet} = 0~1 °C); (b) width of 95% confidence interval for the regression of transition elevation at T_{wet} = 0.5 °C; and (c) lapse rate of T_{wet} during snowfall. The probabilities of shade bands (areas of mean ± standard deviation) are labeled.

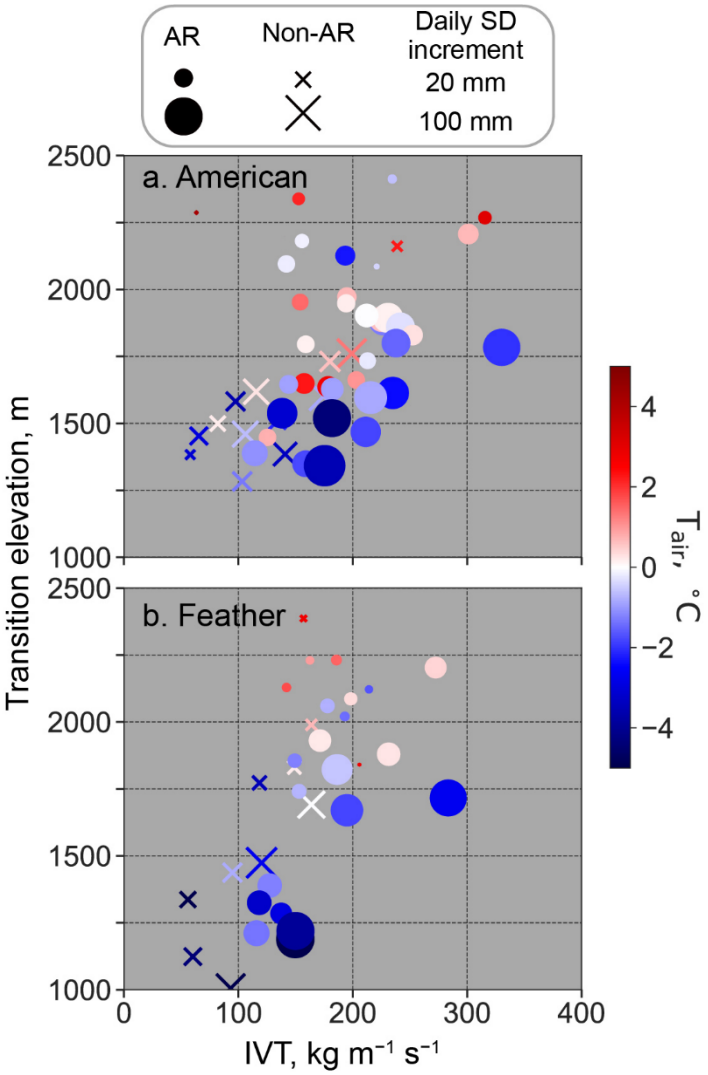

Figure 13. (a) Rain-snow-transition elevation versus basin-averaged T_{air} and mean Integrated water-Vapor Transport (IVT) intensity at Folsom Dam for events in the American River basin WY 2014-17. Panel (b) is the same as (a), but for the Feather River basin WY 2017-18 using IVT at Oroville Dam. Marker size represents basin-averaged daily snow depth increment in events. Atmospheric-river (AR) events are marked using circles and non-atmospheric-river (non-AR) events are shown in x markers.

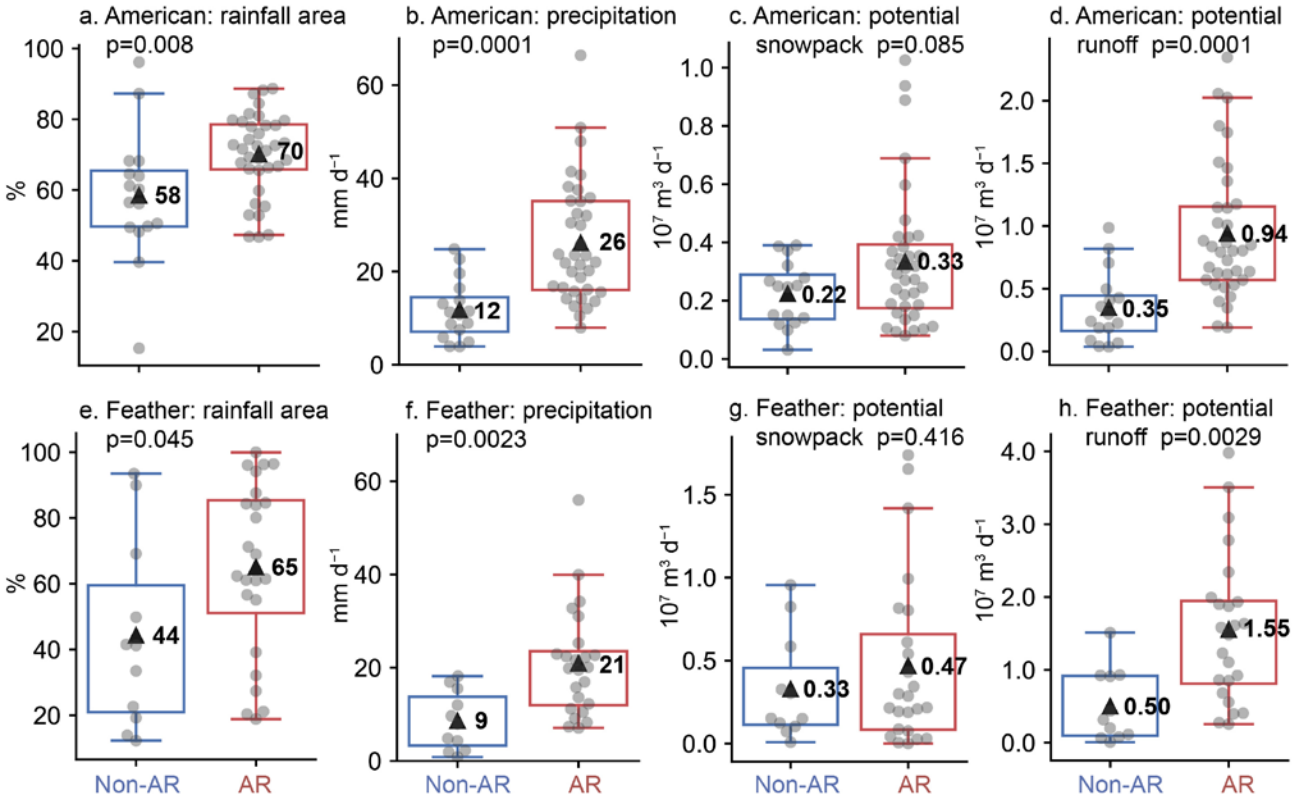

Figure 14. Comparison between atmospheric-river (AR) events and non-atmospheric-river (Non-AR) events in the winter seasons for the American River basin in WY 2014-17: (a) mean rain area below the rain-snow-transition elevation, expressed as percent of the basin area, (b) daily basin-averaged precipitation amount using the PRISM dataset, (c) daily mean potential snowpack volume, and (d) daily mean potential runoff volume. (e-h) are the same as (a-d), but for the Feather River basin in WY 2017-18. The box denotes interquartile range with lower and upper boundaries of 25th and 75th percentiles, respectively, whiskers indicate the 1.5 times of interquartile range beyond the box boundaries, grey dot shows the mean daily value of each event, and the triangle is the average value of the group and labeled as black. The p-value of the T-test is also shown in each panel.

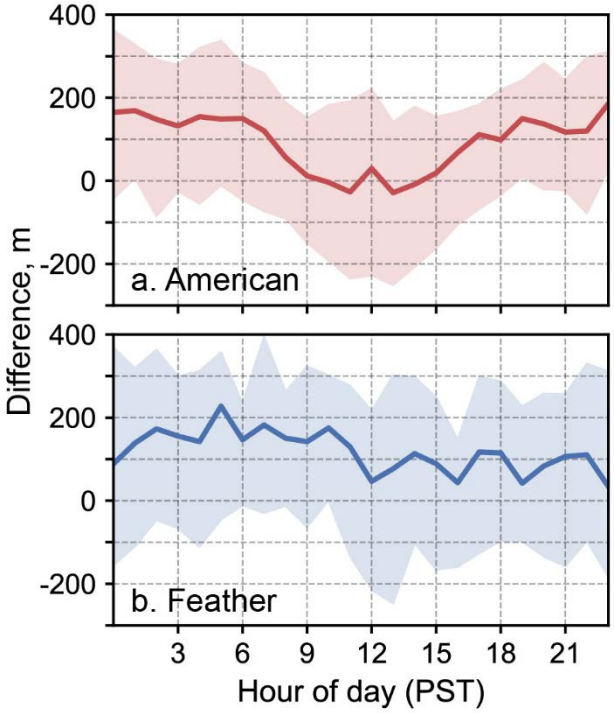

Figure 15. Difference between rain-snow-transition elevation based on T_{wet} = 0.5 °C and radar snow level at each hour of the day (PST): (a) the American River basin WY 2014-17 and (b) the Feather River basin WY 2017-18. Solid line is the mean difference with positive values indicating higher radar snow level than transition elevation from T_{wet}, and shaded areas mean the interquartile between 25% and 75%.

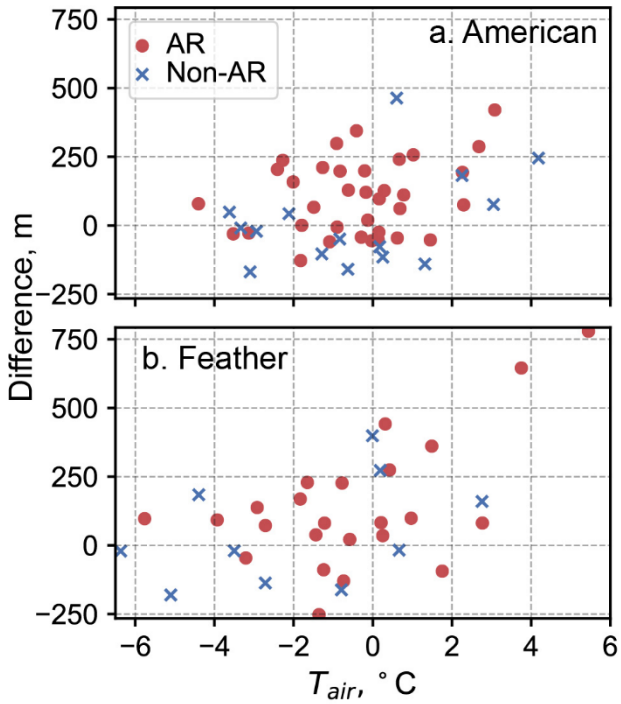

Figure 16. Difference between rain-snow-transition elevation based on T_{wet} = 0.5 °C and radar snow level as a function of basin-averaged T_{air} during the events in (a) the American River basin WY 2014-17 and (b) the Feather River basin WY 2017-18. AR events are marked using circles and non-AR events are shown in x markers. Positive values of difference mean higher radar snow level than transition elevation based on T_{wet}.

Supplemental Material

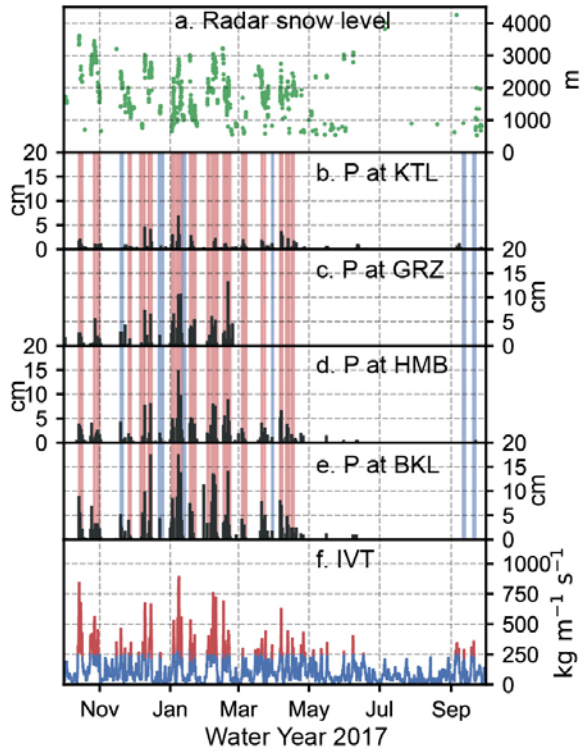

Figure S1. WY 2017 storm events shown using observations in the Feather River basin. (a) hourly FMCW radar-detected atmospheric snow level at Oroville, (b)-(e) show the precipitation (P, black) measured by precipitation gauges at KTL (2206 m), GRZ (2068 m), HMB (2008 m), and BKL (1742 m) sites from CDEC, respectively (Figure 2). Shaded bands indicate selected storm events (Figure 3), red bands for atmospheric-river events and blue bands for non-atmospheric-river events. Panel (f) shows Integrated water-Vapor Transport (IVT) at Oroville Dam, from the MERRA-2 dataset, with intensities larger than a threshold of 250 kg m^{-1} s^{-1} marked as red.

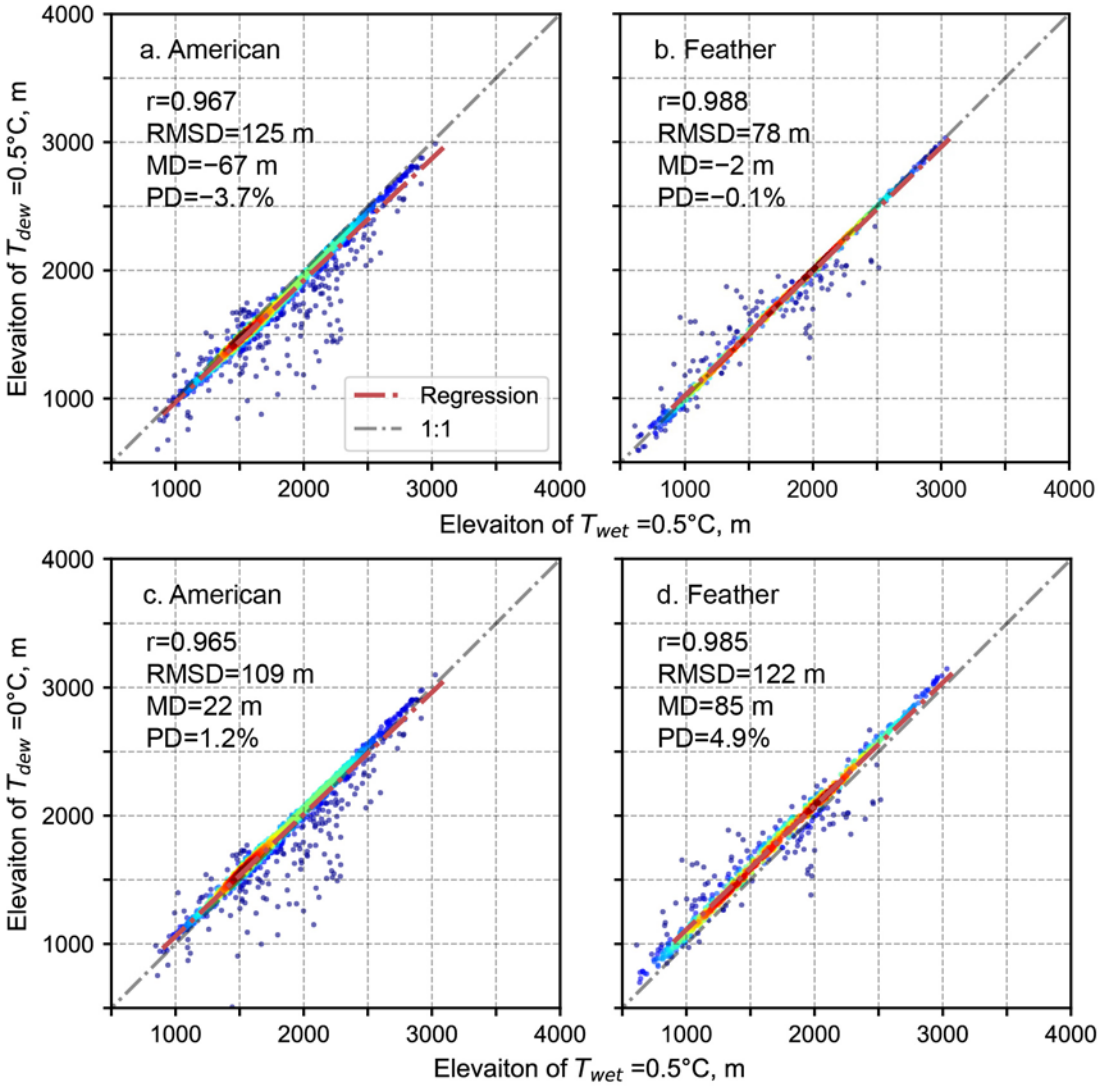

Figure S2. Elevation at T_{wet} = 0.5 °C from the wireless-sensor networks versus elevation at T_{dew} = 0.5 °C during events in November-April: (a) the American River basin for WY 2014-17 and (b) the Feather River basin for WY 2017-18. (c) and (d) are similar to (a) and (b), but show the comparison between elevation at T_{wet} = 0.5 °C and T_{dew} = 0 °C. Red line is the regression line of the dots colored by point density (red for high density and blue for low density). RMSD: root mean squared difference, MD: mean difference, and PD: percent difference.

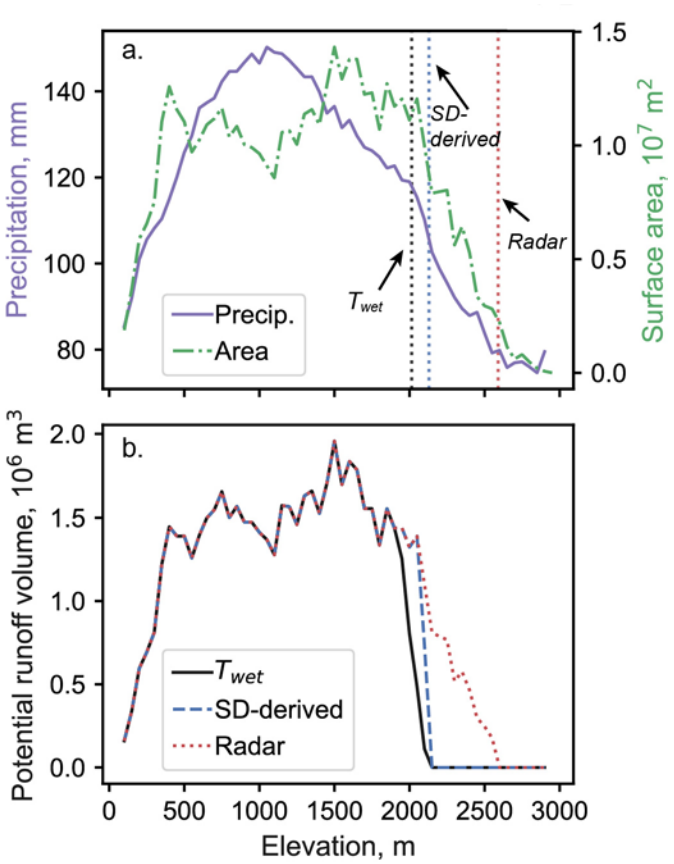

Figure S3. (a) Different rain-snow-transition elevations in the American River basin on February 8, 2014 (Figure 5) from three methods, T_{wet}, ground snow-depth(SD)-derived, and radar, which are shown as vertical dotted lines. Precipitation from the PRISM dataset and surface area are plotted at each elevation bin (50 m); and (b) comparison of potential runoff volume estimates using liquid precipitation (rain) below the transition elevations multiplying contributing area.

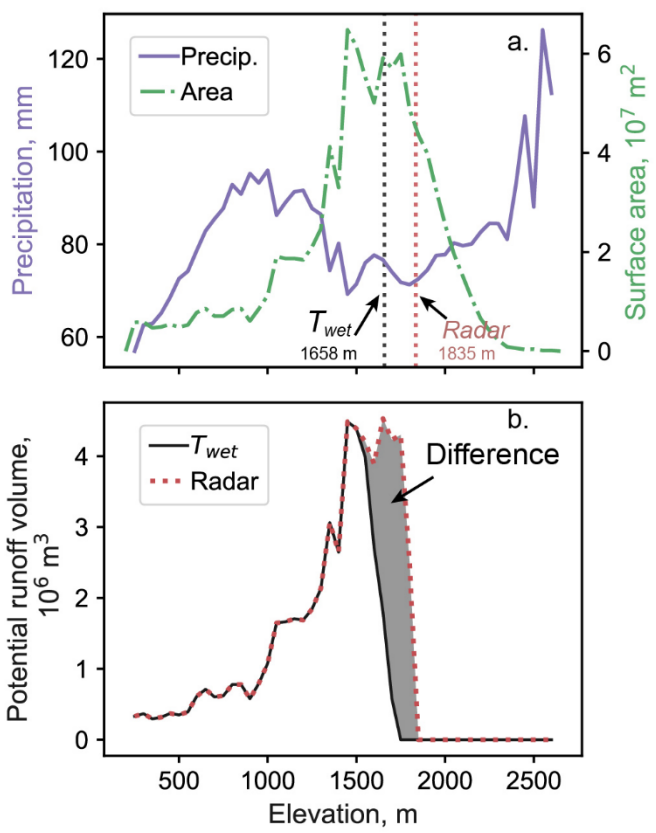

Figure S4. (a) Different rain-snow-transition elevations in the Feather River basin on January 10, 2017 during an atmospheric-river event from two methods, T_{wet} and radar, which are shown as vertical dotted lines; and (b) comparison of potential runoff volume estimates. The difference of potential runoff volume is shown as the grey shaded zone.